Journal of Computational Applied Mechanics 2026, 57(4): 569-596

DOI: 10.22059/jcamech.2026.417785.1874

RESEARCH PAPER

CFD Simulation of Supersonic Combustion and Mixing with Flushwall and Ramp Injection Effects for Scramjet Propulsion

Levi Smith-Hyde [a], O. Anwar Bég [b], Tasveer A. Bég [c], Henry J. Leonard [b], M.M. Bhatti [d,e,*], Ali Kadir [b], Walid S. Jouri [b]

[a] *Component Design Engineer, Rolls Royce plc (Propulsion Division), Moor Lane, Derby, Derbyshire, DE24 8BJ, UK*

[b] *Multi-Physical Engineering Sciences Group, Mechanical Engineering Department, Corrosion and Coatings Lab, Room 3-08, SEE Building, University of Salford, Manchester, M54WT, UK*

[c] *Engineering Mechanics Research, Israfil House, Dickenson Rd., Manchester, M13, UK.*

[d] *Department of Physics, College of Science, Korea University, 145 Anam-ro, Seongbuk-gu, Seoul 02841, Republic of Korea*

[e] *Material Science Innovation and Modelling (MaSIM) Research Focus Area, North-West University (Mafikeng Campus), Private Bag X2046, Mmabatho 2735, South Africa*

Abstract

Scramjet technology promises to reduce the cost of space access systems by eliminating rocket staging designs to reach orbit which are costly and single use. To date, several Scramjet engine testbeds have been capable of igniting and producing thrust in flight conditions, but these tests are not common. Scramjet propulsion systems are faced with complex flow-physics behaviours that moderate their technological development. The insufficient knowledge available on restricted sonic airflow conditions requires computational methods for accurate predictions prior to flight testing. This article therefore deploys ANSYS FLUENT Computational Fluid Dynamic (CFD) software to analyse supersonic flow characteristics in current scramjet combustor designs. The scope of flow passage optimisation in Scramjets lies primarily with the selected fuel injection methods and in this regard both flush wall (30 degrees and 80 degrees inclination) and ramp injector (12 degrees and 18 degrees inclination) designs are simulated here. Reynolds Averaged Navier Stokes (RANS) computations are described to provide numerical results for high velocity, recirculating flows and static pressure, temperature, velocity, density and hydrogen/water/oxygen mass fraction contours are presented. Detailed mesh designs are included and a grid independence study. The material properties of air and the mixture (hydrogen-air) feature ideal-gas density and Sutherland's viscosity for heat transfer properties to accurately simulate compressibility effects. A two equation, realizable k-epsilon turbulence model is employed with standard wall treatment, to encompass superior simulated rotational spreading behaviour of the flow. The Turbulent Kinetic Energy (TKE), Energy and Wall Prandtl numbers are set as 1, 0.85, and 0.85 respectively. To model the mixing, heat transfer, and combustion with

* Corresponding author. Tel.: +0-000-000-0000 ; fax: +0-000-000-0000 .
E-mail address: mmbhatti@korea.ac.kr

the realizable k-epsilon model, a volumetric, hydrogen-air mixture Species-Transport model with Eddy-Dissipation turbulence-chemistry interactions is incorporated with turbulent Schmidt number of 0.7 and a Turbulent Dissipation Rate (TDR) of 1.2. Two distinct fuel injection methods are presented in this study- the transverse flush wall injection and the ramp method. The hydrogen fuel is injected through a port with a 2mm cross-sectional area. The ramp injection method is an intrusive fuel injection method which trades thrust potential in the form of pressure losses for good mixing characteristics. The strength of the oblique shockwave that forms is entirely dependent on the inclination of ramp, with greater inclination resulting in a stronger shockwave. The presence of the oblique shockwave further increases the mixing downstream of fuel injection due to the interaction of reflected shockwaves with the fuel and air mixing layer. Similar to the flush wall injectors, both ramp designs feature fuel injection ports of 2mm diameter, where the opening of the injector port is 2mm below the upper trailing edge of the ramp geometry. The 18° ramp, due to its high profile, generates strong oblique shockwave formation and enhanced downstream mixing due to increased pressure and temperature due the reflection of the intense oblique shock. The 80° flush wall injector features the same general dimensions as the first case at 30° inclination but introduces the hydrogen fuel near perpendicular to the airflow.

Keywords: Scramjet propulsion; flush wall; ramp; injectors; mixing; shocks; CFD; combustion

1. Introduction

Conventionally, contemporary aircraft propulsion systems are embodied by an air inlet, a series of complex high rotational-velocity fan and compressor stages, isolated combustion chambers, turbine stages, and an exhaust. Since their conception and widespread application from the early 1960's, turbojet, turbofan, and turboramjet designs have now reached a stage of perpetual optimisation. The limits of propulsive capability have been reached and to travel further, and faster, new engine designs such as scramjet engines embody the next frontier of propulsive technologies. Scramjet designs [1] use the forward geometry and velocity of an aircraft to appropriately condition the compression of oncoming air for combustion, eliminating the requirement for a complex series of rotational compressor stages with conventional designs. The accomplishment of such a propulsion method would enable travel at extreme velocities from Mach 2 to in excess of Mach 12 and higher. One of the longest routes operable across the globe today is from London Heathrow in the United Kingdom to Sydney, Australia, which takes approximately 20 hours across a distance of ~17,000km. The true benefits of hypersonic flight made possible by scramjet propulsion systems becomes clear when recognising the same flight would take just 2.5 hours for a hypersonic vehicle travelling at the fastest experimentally demonstrated speed of Mach 6. Scramjet systems provide a means through which cross-planetary travel times can be greatly reduced [2]. In addition to transport, access to space is also promised by engine designs such as the SABRE which is a dual-mode engine concept that proposes a design that incorporates ramjet and rocket technology for atmospheric and space flight. The current scope of scramjet propulsion design research encompasses flow path optimisation for enhanced combustion efficiency. Combustion efficiency is the key defining factor affecting the implementation of scramjet propulsion designs as distinct injection methods have varying effects on thrust production over a wide range of flight speeds. Due to the high velocity flow regimes within an operating scramjet, the residence times of fuel and air through a given control volume is very low, exacerbating effective mixing of the air and fuel for combustion. Mixing efficiency governs the effectiveness of combustive processes that take place in the combustor and as such embody a significant proportion of the research done to date. In parallel with experimental testing, numerical simulation has emerged as a major tool in evaluating possible designs for improved mixing and combustion efficiency in scramjet propulsion systems. Both methodologies have provided important insights into optimizing mixing and combustion characteristics. Drozda et al. [3] computed the mixing characteristics of several fuel injectors under hypersonic flow conditions. The study used the Vulcan-CFD solver and Reynolds-Averaged Simulations (RAS) method to correspond to NASA Langley's Enhanced Injection and Mixing Project (EIMP) at Mach 6.4. Analysis was conducted on 3 injector types- fuel placement (strut), fluidic vortical mixer (ramp) and flush wall injector for comparison. They provided excellent benchmarks characterising the flow behaviour and effects of distinct injectors in hypersonic flow and elaborated on the trade-offs that can be made in the combustor design process. The strut injector produced the greatest amount of mixing at the expense of total pressure loss due to its highly intrusive presence in the flow. The flush wall injector

produced least mixing but greatest specific thrust potential due to large dynamic pressure, resulting from its minimal intrusive geometrical impact on the flow. The mixing efficiency of the strut and ramp were found to be comparable. The flush wall injector however introduced a significant amount of fuel into boundary layer and sustained high Mach flow further aft of the combustor. Fuel and air mixed fastest for the strut injector, followed by the ramp, and the flush wall injectors, suggesting that while the flush wall injectors display highest Mach flow, they provide minimum mixing of the air and fuel, resulting in a significantly lower combustion and mixing efficiency. It was found that, in general greater mixing resulted in greater amounts of total pressure loss, in the case of the strut injector, due to the large surface area exposed to the oncoming flow. Drozda et al. [4] examined the effects of flush wall injectors for scramjet applications using a Latin hypercube sampling process that specified design points for the Reynolds Averaged Simulations (RAS). Thrust potential and combustion efficiency were selected as the critical design elements for optimisation. An automated methodology was devised to build geometries and grids for each design of injector. Both of the specified optimisation parameters were found to be driven by duct height by extensive computational methods. The results were obtained by utilising a Viscous Upwind algorithm for complex flow analysis in Vulcan-CFD with structured multiblock grids. The turbulence model used was the Menter baseline two-equation turbulent physics model. Reynolds heat and species mass flux were modelled using a gradient diffusion model and turbulent Prandtl was deployed as 0.9, and Schmidt number at 0.5. The findings indicated that the increase of duct height increases thrust potential and decreasing duct height results in an increased combustion efficiency. Therefore, duct height can be a useful variable of design. Increased injector angles (tending to 90 degrees) were shown to decrease thrust potential and increases combustion efficiency. High angle injection however was noted to subtract from the streamwise flow momentum and contributed more to the mixing and therefore combustion efficiency due to stronger bow shock flow vorticity effects. A lower injection angle therefore was emphasized to increase thrust potential due to additional contribution to axial flow. However, a low angle of injection was not able to achieve a comparable combustion efficiency or good levels of fuel diffusivity over the combustor cross-sectional area, despite reduced pressure losses. It was further noted that flush wall injection requires angular compromise to achieve desired efficiency/combustion. Bouazzi et al. [5] used ANSYS FLUENT finite volume method (FVM) software to simulate the effects of multiple injectors positioned behind a ramp in scramjet combustors and to compare fuel jet interactions and penetration of four jets placed behind the ramp under supersonic flow conditions. They compared one-sided and two-sided configurations to elucidate effective mechanisms of fuel jet mixing and observed that while the two-sided injection improves the fuel jet strength, the one-sided injection achieves enhanced fuel mixing efficiency within the supersonic combustion chamber (18% greater than that from the two-sided jet downstream of the ramp jet). Dharan et al. [6] used Schlieren imaging and PLIF imaging to study supersonic mixing characteristics of an internal cross flow effervescent ramp injector in a scramjet and mixing time. They considered a modified ramp injector such that the fuel stream is impinged by a secondary jet prior to fuel injection and compared supersonic cold flow mixing of the modified internal cross flow ramp with the baseline standard ramp configuration. They observed that in the vicinity of the injector, the modified ramp achieves superior fuel stream spread relative to the pure liquid injection. They also noted that effervescent injection sustains a higher fuel spread and, substantially elevated atomization rate compared to pure liquid injection. Omar et al. [7] used non-reactive RANS CFD simulations to investigate the compressible air flow near a scramjet ramp injector with double circular injectors for fuel mixing and fuel jet penetration of hydrogen jets for two injector configurations at free stream Mach number of 2. They studied the impact of nozzle space on the fuel distribution and mixing mechanisms and noted that larger jet space produces higher circulation strength. They also showed that mixing efficiency of the model with low jet space is improved as the dual jet interaction influences diffusion and mixing inside the combustion chamber. Jacobsen et al. [8] described supersonic wind tunnel studies of simplified and revised multiport aerodynamic-ramp injector arrays in a supersonic flow. They deployed four flush-walled holes for test conditions of sonic air injection into a Mach 2.4 air cross stream with an average Reynolds number of 42 million with jet-to-freestream momentum flux ratios from 1.1 to 3.3. They generated shadowgraphs and surface oil-flow visualization pictures close to the injectors to establish the injector flow field characteristics. The mixing characteristics of the injectors at three downstream stations were measured with total temperature probes and it was observed that aerodynamic-ramp mixed faster and produced a greater plume area relative to the single-hole injector, although it exhibited greater pressure losses as a result of higher downstream-angled injector arrangement and elevated impedance. Swain et al. [9] studied computationally the performance of a novel asymmetric strut-based fuel injection design for enhanced fuel-air mixing and supersonic combustion. They showed that asymmetry in the strut produces vortices along the longitudinal direction after the flow crosses over the lip of the strut, and this enhances circulation in the downstream of the combustor and elevates the air and fuel mixing and combustion efficiency. Abdelhameed et al. [10] used OPENFOAM CFD software, Reynolds-Averaged Navier-Stokes (RANS) equations, the Shear Stress Transport (SST) turbulence model, and the energy equation, to simulate hydrogen fuel mixing in a scramjet cold flow regime. They considered chemical reaction effects and computed mixing efficiency and total

pressure loss for various engine geometries, including cavity, strut-cavity, and double-cavity-strut configurations. They found that shockwave interactions strongly modify flow dynamics, with the strut-cavity configuration producing the best fuel diffusion and mixing efficiency. Hu et al. [11] investigated flush wall in supersonic incoming air flow at Mach number of 3 with liquid kerosene as the fuel. They measured the combustion performance and wall temperature gradients at various fuel feeding ratios between the wall and the strut and noted for a constant equivalence ratio and fixed axial injection position, there is a strong influence of strut/wall fuel feeding ratio. They also noted that the best combustion performance was achieved with strut only injection and the average distributed strut/wall injection modes, although the latter achieves a reduced wall temperature gradient attributable to strong film cooling. Hou et al. [12] conducted 3-dimensional CFD simulations of reactive supersonic mixing and combustion in a staged supersonic combustor. They simulated a swept ramp injector as the second-stage wall injection mechanism combined with the first-stage central strut injection in order to produce optimum stream-wise vortices, noting that two-staged injections more effectively utilize residual oxygen near the wall and release more heat. The second-stage injection further downstream was found to mitigate strong shock waves in the isolator and achieved ascending wall pressure and efficient burning after the wall injection, maximizing the quantity of fuel to injected into the supersonic combustor without thermal choking. Kummitha and Pandey [13] investigated numerically the influence of a wavy (corrugated) wall strut fuel injector on shock wave development, shear mixing and streamline vortex development in scramjet combustion at different flow conditions (Mach numbers of 2, 4 and 6). They deployed the SST k-ω turbulence model and observed an increase in the quantity of oblique shock waves and turbulence intensity with the wavy wall strut fuel injector. They concluded that the wavy wall strut significantly improves the shock-induced blend augmentation of fuel and air. Donohue et al. [14] deployed the SPARK 3D Navier-Stokes computer code and planar laser-induced iodine fluorescence (PLIIF) techniques to study the time-averaged pressure, temperature, velocity, and injectant mole fraction in supersonic flow around a swept ramp fuel injector. They noted that weak asymmetry in the incoming flow is magnified by boundary layer separation arising due to the reflection of the ramp generated shock from the duct walls. Bogdanoff [15] has also provided a good survey of different injection methods for improving combustion efficiency in scramjet systems. Another excellent survey of the area has been conducted by Rubins and Bauer [16]. Other interesting articles have been communicated by Masuya et al. [17] for fuel injection struts, Mitani et al. [18] for chemical reaction effects in scramjet combustion and Houria et al. [19] (for hydrogen jet fuel injection with struts).

Efficient fuel–air mixing remains one of the primary challenges in supersonic combustion chambers due to extremely short residence times and strong compressibility effects. The previous investigations have not addressed exhaustively different injection angles for ramp or flush wall injector designs. In the current study, we therefore present detailed CFD simulations to suggest optimisations to the current design challenges regarding the mixing and combustion efficiency effects of distinct fuel injector designs. The importance of research on this topic comes at an exciting time for aerospace vehicles as the commercial space industry is growing rapidly, as well as implementation of new and well-backed supersonic transport projects. With commercial projects in the 21st century promoting the use of supersonic aircraft, a new page has been turned in the history of the development of aircraft, one that will ultimately lead to more advanced research, systems, and advent of scramjet propulsion implementation. ANSYS FLUENT turbulent RANS simulations are conducted for the investigation of scramjet combustor flow phenomena. Computational results are provided for static pressure, velocity, static temperature, density, combustion mass fractions (hydrogen, water and oxygen) with different configurations for flush wall and ramp injection methods in supersonic flow. The simulated results are correlated with previous studies where possible Ramp injection methods are found to exhibit ideal mixing and combustive characteristics.

2. Flow physics models

A functioning scramjet system is an integration of multiple mechanical, electrical and aerothermodynamic design disciplines, often operating at the peak of their respective capabilities. Here the primary focus is on aerothermodynamic analysis of the internal flows. Initially, the presence of shock structures for the inlet aerothermodynamics will be the first effect to be encountered, followed by the internal flow behaviour that governs the quality and effectiveness of mixing and combustion. Distinct from a typical jet engine cycle, the scramjet engine type has a specific set of stations to embody the primary components in the design of a supersonic combustion system. The general configuration of modern scramjets is shown in Fig. 1 and adapted from Hirschel et al. [20]. The compressibility effects observed in scramjet combustors in the form of shockwaves and fluctuations in fluid density are primary drivers of mixing and combustion enhancement. The effects of the strong shockwaves presented upon interaction with the fuel-air layer indicates that the flow experiences shock-induced combustion. The phenomenon of shock-induced combustion has been extensively studied- see for example Rubins and Bauer [16] and is characterised by an increase in temperature and mixing upon interaction of a strong reflected shockwave and a fuel-air mixing layer. Prior to the stages of fuel injection which are the primary focus of this article, the flow on an

operational scramjet design is conditioned by the geometry of the engine inlet. The geometric layout of the inlet, due to the freestream velocity, will introduce a system of shockwaves according to the angular characteristics upstream of the combustor. Due to this behaviour in the super/hypersonic flow regimes, a consideration for the relevant aerothermodynamic behaviour is required.

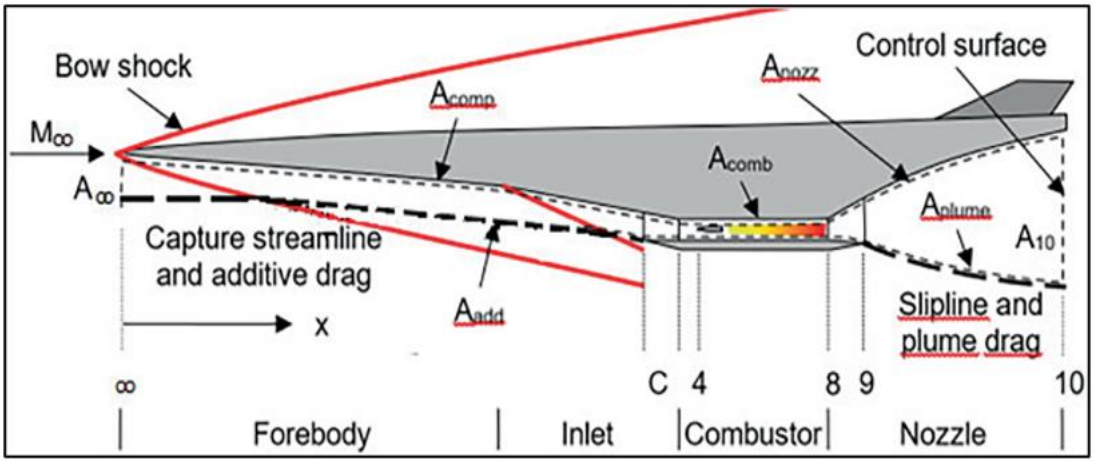

Fig 1: Scramjet propulsion system with airframe-propulsion integration (API)

2.1. Navier-Stokes model

The Navier-Stokes equations are utilized to simulate the regime. These partial differential equations can be solved to describe the aerothermodynamic behaviour of air-fuel systems in terms of velocity, temperature, energy, pressure, and density. ANSYS Fluent [21] employs Reynolds-Averaged Navier-Stokes (RANS) solution methods for turbulent flows, whereby the solver averages the flow variations over a given period of time, resulting in distinct mean-flow quantities and turbulence fluctuation calculation. The time-averaged turbulent flow is sufficiently accurate for analysing internal (propulsion duct) flows, though due to the nature of the method, exact simulations can never be produced, requiring infinite computing power on an exponential scale to achieve near-perfect flow characterisation. Compressible turbulent, supersonic aerodynamic flow, with constant atmospheric pressure and no slip at the duct internal body walls is considered. The governing equations, i.e. Navier-Stokes equations take the form of the continuity and momentum conservation equations:

$$\frac{\partial \rho}{\partial t} + \nabla \rho v = 0, \tag{1}$$

$$\rho\left(\frac{\partial v}{\partial t} + v\nabla v\right) = -\nabla p + \mu \nabla^2 v, \tag{2}$$

Here ρ is the fluid density (kg/m^3), v is the velocity field vector (m/s), t is the time (s), p is the pressure field (N/m^2), μ is the dynamic viscosity of the fluid ($kg/m\ s$). For 2-dimensional axisymmetric gas dynamic duct flow, as considered here, *(u, v) are velocity components (m/s) in the axial (x) and transverse (y) directions, respectively, x is the axial (longitudinal) coordinate, and y is the transverse coordinate.*

2.2. k-epsilon Turbulence Model

The k-epsilon turbulence model is deployed which achieves reasonable accuracy in high-speed gas dynamic internal flows and furnishes adequate refinement in the velocity field and simultaneously avoids excessive compilation times required with alternate turbulence models (e.g. RNG, LES). The k-epsilon model describes the level of transport facilitated by the turbulent behaviour of the fluid and satisfy the stress tensor encountered in the momentum equations. Additionally, and notably, specific to the study of internal flows in this paper, the model also defines additional terms for production, transport and dissipation, accounting for fluctuating turbulent effects in the time-averaged flow solutions. The standard k-epsilon turbulence is the most common Reynolds Averaged Navier Stokes (RANS), two-equation, semi-empirical model which is based on the following transport equations for turbulent kinetic energy, k and its dissipation rate ε:

$$\frac{\partial}{\partial t}(k\rho) + \frac{\partial}{\partial x_i}(k\rho u_i) = \frac{\partial}{\partial x_j}\left[\left(\mu + \frac{\mu_t}{\sigma_k}\right)\frac{\partial k}{\partial x_j}\right] + G_k + G_b - \rho\varepsilon - Y_M + S_k, \tag{3}$$

$$\frac{\partial}{\partial t}(\varepsilon\rho)+\frac{\partial}{\partial x_i}(\varepsilon\rho u_i)=\frac{\partial}{\partial x_j}\left[\left(\mu+\frac{\mu_t}{\sigma_\varepsilon}\right)\frac{\partial\varepsilon}{\partial x_j}\right]+C_{1\varepsilon}\frac{\varepsilon}{k}(G_k+C_{3\varepsilon}G_b)-C_{2\varepsilon}\rho\frac{\varepsilon^2}{k}+S_\varepsilon. \quad (4)$$

The production and destruction of turbulent kinetic energy are always closely linked- the rate of dissipation is large where the rate of production is large. Here G_k = turbulence kinetic energy generation due to mean velocity gradients, G_b is the generation of turbulence kinetic energy due to buoyancy, Y_M is the contribution of the fluctuating dilatation in compressible turbulence to the overall dissipation rate, $C_{1\varepsilon}, C_{2\varepsilon}, C_{3\varepsilon}$ are constants, σ_k and σ_ε are turbulent Prandtl numbers for k and ε respectively, with values of 1.0 and 1.3 and S_k and S_ε are user-defined source terms. To determine turbulent length and time scale, we deployed test values of 0.05-0.07 times the characteristic length (duct width) for the turbulent length scale and turbulent intensity was tested between 1-10%. *k and* $\boldsymbol{\varepsilon}$ are then determined from these more specifically since in ANSYS FLUENT [21], the default *k=1 and ε=1*, are often too high. Dissipation rate (ε) was adjusted to match the length scale and prevent premature decay of turbulence. The constants $C_{1\varepsilon}, C_{2\varepsilon}, C_{3\varepsilon}$ were prescribed values of 1.44, 1.92, 0.09, values which are widely accepted for gas dynamics flows [22]. The *k*-epsilon model assumes that the flow is fully turbulent with the effects of molecular viscosity negligible. The *k*-epsilon turbulence model is however only valid for fully turbulent flows and performs poorly when simulating flows with strong separation, high pressure gradients and very large streamline curvature.

2.3. Energy Equation

The energy equation embodies the conservation of energy principle, defining the quantitate variations in total energy due to convective and diffusive in addition to work done by body and pressure forces.

$$\frac{\partial(\rho E)}{\partial t}+\nabla\cdot(\rho u E)=\nabla\cdot(k\nabla T)+\nabla\cdot(\mu_t u\cdot u)-p\nabla\cdot u \quad (5)$$

Here E =Total energy per unit mass (internal energy plus kinetic energy) *(J/kg),* T *=static emperature (K),* k *=thermal conductivity (W/mK),* μ_t *=turbulent viscosity (Pa.s),* $\dot{q}$ *=Heat source/(sink term), u is velocity (m/s).*

2.4. Sutherland's Viscosity Law

Sutherland's viscosity is utilised in the ANSYS Fluent simulations described in due course to account for thermal effects on fluid viscosity. The law is rooted in the kinetic theory of the ideal gas law and intermolecular force potential.

$$\mu=\mu_{ref}\left(\frac{T}{T_{ref}}\right)^{\frac{3}{2}}\frac{T_{ref}+S}{T+S} \quad (6)$$

Here T =Absolute Temperature $[K]$, T_{ref} =Reference Temperature $[K]$, μ_{ref} =dynamic viscosity at T_{ref} and S = Sutherland's temperature coefficient = $[110.4K]$ for Air.

2.5. Fuel

The primary fuel subject to research for scramjet engines is gaseous hydrogen (H_2). Ultimately, H_2 has two critical benefits over other fuels, namely wide flammability range and high energy release per unit burn. It is essential to highlight the characteristics of viable design options for a combustible fuel. As such, Table 1 highlights four fuel options that can be considered for selection as a combustive fuel. Overall, H_2 is seen to have the best properties as a combustive fuel but requires additional considerations for storage due to its low density.

Table 1: Scramjet fuel considerations

Scramjet Fuel Consideration		
Fuel Type	**Advantages**	**Disadvantages**
H2 - Gaseous	High Calorific Value (120MJ/kg), High Diffusivity, Wide Flammability Limits	Low Density
N2 - Gaseous	High Diffusivity	Low Calorific Value (52MJ/kg), Narrow Flammability Limits, Low Density
C2H4 - Gaseous (Hydrocarbons)	Wide Flammability Limits, High Density	Low Calorific Value (45MJ/kg)
Kerosene - Liquid	High Density	Low Calorific Value (45MJ/kg), Narrow Flammability Limit

A sample calculation of the Prandtl number is presented below for gaseous hydrogen at a temperature of 873K, at atmospheric pressure. The selection of gaseous hydrogen represents a typical Scramjet injector fuel.

$$Pr = \frac{C_p \mu}{k} = \frac{\mu/\rho}{k(C_p \rho)} \tag{7}$$

For gaseous hydrogen, specific heat capacity, $C_p = 14{,}800\ (J/kg \cdot K)$, dynamic viscosity $\mu = 0.0000184\ (kg/m \cdot s)$ and thermal conductivity $k = 0.412\ (W/m \cdot K)$. This gives $Pr \approx 0.66$ which falls within expected values and indicates that the gaseous hydrogen has relatively high thermally diffusive behaviour compared with its momentum diffusivity. This means that hydrogen has a good balance between heat conduction and ability to transfer momentum.

3. Ansys fluent CFD simulations

3.1. Geometric designs studied

Two distinct fuel injection methods are simulated- transverse flush wall injection and ramp injection. The combustor features an overall length of 800mm and height of 150mm in all cases. The flush wall injection method is a non-intrusive method of fuel injection, whereby fuel is injected from a simple port at the wall. Combustors that utilise a flush wall injection type will see the highest specific thrust potential due to the large dynamic pressure that occurs due to minimal intrusion into the flow and as such are a highly frequent choice for scramjet combustor designs. However, while the flush wall injectors have the highest specific thrust potential, due to the high velocity of the oncoming freestream air, it is established now that flush wall injection methods generally yield the lowest amount of fuel-air mixing, resulting in a lower value of achieved thrust due to inadequate diffusion of the fuel with the air for useful combustion. The first and second simulation cases are for a flush wall injector with a 30˚ inclination and then 80 ˚ inclination to the flow direction as presented in Figure 2 with relevant dimensions.

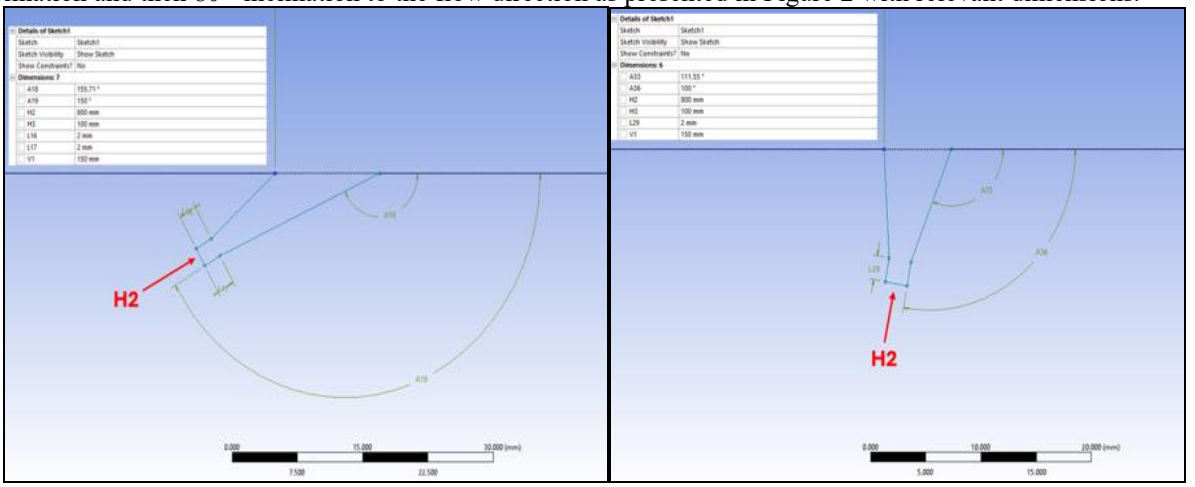

(a) **(b)**

Fig 2: a) 30˚ Flush wall injector geometry b) 80˚ Flush wall injector geometry

The hydrogen fuel is injected through a port with a 2mm cross-sectional area with the boundary conditions presented later. Typically, the flush wall injection method will see a bow shockwave formation at the point where the supersonic air stream meets the supersonic hydrogen injection. Due to the high velocity of the fuel and air, it is most likely that due to the profile of the first case (Fig 2a), at 30˚, the majority of the injected fuel will be introduced into the boundary layer and promote minimal mixing. With high thrust potential due to dynamic pressure, the flush wall method is essential to optimising future scramjet designs and as such, an increased inclination of 80˚ is presented for the second case (Fig 2b). The 80˚ flush wall injector features the same general dimensions as the first case at 30˚ inclination but introduces the hydrogen fuel near perpendicular to the airflow. Due to the minimal mixing characteristics of the flush wall injection method, increasing the inclination of the supersonic fuel injection will likely decrease the amount of fuel introduced into the boundary layer, providing a more effective mixture for combustion while maintaining high dynamic pressure thrust potential. Increasing the inclination of fuel injection into supersonic flow enables a larger effective area of the combustor cross-sectional area to diffuse air and fuel.

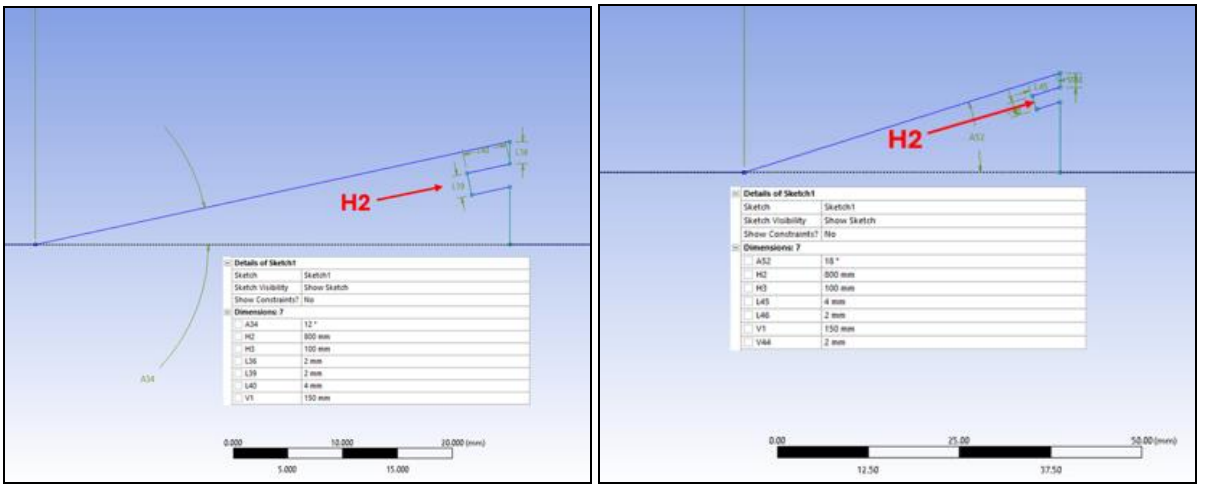

(a) **(b)**

Fig 3: a) 12˚ Ramp injector geometry, b) 18˚ ramp injector geometry

The *third and fourth cases* examined, as presented in Figure 3 a, b correspond to the ramp injection method. The ramp injection method is an intrusive fuel injection method which trades thrust potential in the form of pressure losses for good mixing characteristics. Due to the high surface area presented to the flow for intrusive injectors in the form of ramps and struts, a significant pressure loss is encountered which limits the downstream capability of the combustor. It is known that pressure degradation, maximised in the case of intrusive devices can be attributed to extreme frictional losses and the release of heat in accordance with Rayleigh's law. However, the pressure losses encountered by intrusive devices are heavily balanced with the significant mixing characteristics that are introduced by a geometric formation in the path of the supersonic air flow. The high velocity air stream that passes over the region of elevated injected fuel introduces rotational momentum to the flow due to top layer shear forces, resulting in the production of high velocity vortices which greatly enhance the mixing and diffusion of the fuel and air. Furthermore, the positive angular deflection of the ramp results in the formation of an oblique shock wave to change the direction of the flow. The strength of the oblique shockwave that forms is entirely dependent on the inclination of ramp, with greater inclination resulting in a stronger shockwave. The presence of the oblique shockwave further increases the mixing downstream of fuel injection due to the interaction of reflected shockwaves with the fuel and air mixing layer. As a result, the ramp injection cases feature a) 12˚ and b) 18˚ ramp inclinations. Similar to the flush wall injectors, both ramp designs feature fuel injection ports of 2mm diameter, where the opening of the injector port is 2mm below the upper trailing edge of the ramp geometry. The 18˚ ramp, due to its high profile, is expected to feature a strong oblique shockwave formation and enhanced downstream mixing due to increased pressure and temperature due the reflection of the intense oblique shock.

3.2. Mesh Designs

A mesh was constructed for each geometry based on the expected mixing and transport characteristics. For all the generated mesh, a face split was applied to surface geometries to allow higher mesh density to be applied at areas of interest and necessity in the flow. To accurately simulate flow behaviours, higher mesh densities are applied to areas where rotational flows are likely to be encountered such as downstream of the fuel injection, reflecting shockwave regions, and areas where combustion may take place.

Figure 4 depicts the basic mesh settings of each injector case. 4-node quadrilateral elements were used. Table 2 documents the nodes and elements quantity for each mesh for each of the 4 cases simulated. The case with the smallest quantity of elements is Case 1 with the 30˚ flush wall injector, with 276,964 elements. The case with the highest quantity of elements is Case 4 with the 18˚ ramp injector with 459,784 elements. The From the first to last case, the quantity of elements increases to account for the higher resolution of mesh for more complex rotational and mixing flow behaviours. The flushwall injectors feature minimal mixing behaviours resulting in a higher density of mesh just along the axis of fuel introduction. Adversely, the ramp injection method requires a highly dense mesh for accurate simulation of results due to high rotational flow and mixing. These mesh designs were optimized after a detailed mesh independence study.

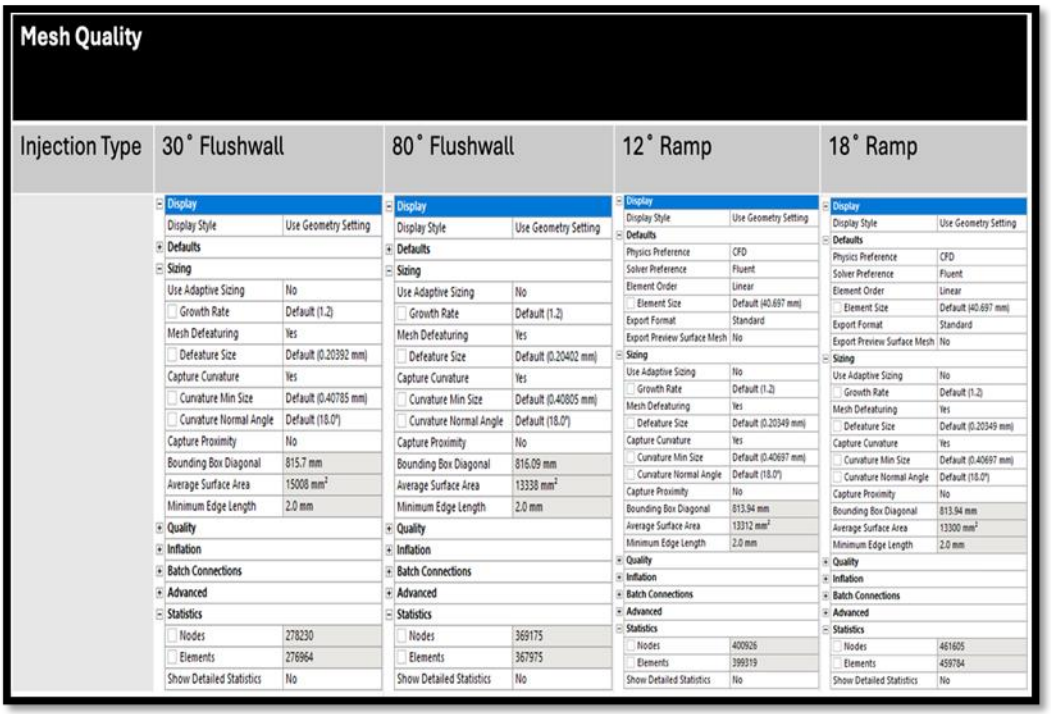

Fig 4: Mesh Quality for all 4 mesh designs for the 4 cases simulated

Table 2: Mesh Element and Node Quantity

Mesh Quality				
Elements	30° Flushwall	80° Flushwall	12° Ramp	18° Ramp
Nodes	278,230	369,175	400,926	461,605
Elements	276,964	367,975	399,319	459,784

The meshes generated for each case are presented in **Fig 5 a)-d)** below.

3.3. Boundary conditions

The specific boundary conditions applied to each of the 4 simulated cases are presented in Table 3, subject to the simulation setup laid out on the next section. The inlet pressure of 100kPa is selected, simulating an environment conditioned by inlet shockwaves which can be configured according to the method laid out in the inlet shock theory section. The flow velocities selected for analysis demonstrates a combustor that is subject to a Mach 2 supersonic freestream for analysis of supersonic aerothermodynamic flow characteristics of distinct fuel injection methods. Hydrogen fuel is injected at Mach 1, noting that increased Mach numbers would require enhancement in terms of pumps and injection methods. Most notably, the species proportions define the quantity of distinct species present in the mixture for subsequent analysis. Approximate atmospheric proportions are outlined in the form of species distributions of nitrogen, oxygen, water vapour, and hydrogen made available by the ANSYS fluent software setup. The simulations assume pure hydrogen injection at a unit value of 1 for the fuel inlet mixture of hydrogen.

3.4. ANSYS Solver Setup

The computations are executed in the density-based solver in ANSYS Fluent software for flow, heat transfer and combustion (species). The software employs the Reynolds Averaged Navier Stokes (RANS) solution method to provide numerical results for high velocity, recirculate flow calculation. The material properties of air and the mixture (hydrogen-air) feature ideal-gas density and Sutherland's viscosity for heat transfer [23] properties to accurately simulate compressibility effects. A two equation, realizable k-epsilon turbulence model is employed with standard wall treatment, to encompass superior simulated rotational spreading behaviour of the flow. The Turbulent Kinetic Energy (TKE), Energy and turbulent Prandtl numbers are set as 1, 0.85, and 0.85 respectively. To model the mixing, heat transfer, and combustion with the realizable k-epsilon model, a volumetric, hydrogen-air mixture Species-Transport model with Eddy-Dissipation turbulence-chemistry interactions is incorporated with Turbulent

Schmidt number of 0.7 and a Turbulent Dissipation Rate (TDR) of 1.2. Table 4 summarizes the methodology. The simulations results obtained are evaluated by observing four primary flow variables throughout the length of the combustor, namely *static pressure, velocity, density and static temperature.* Static pressure and density contours assist in detailed numerical visualisation of shockwave patterns throughout the combustor due to abrupt changes according to oblique shockwave theory.

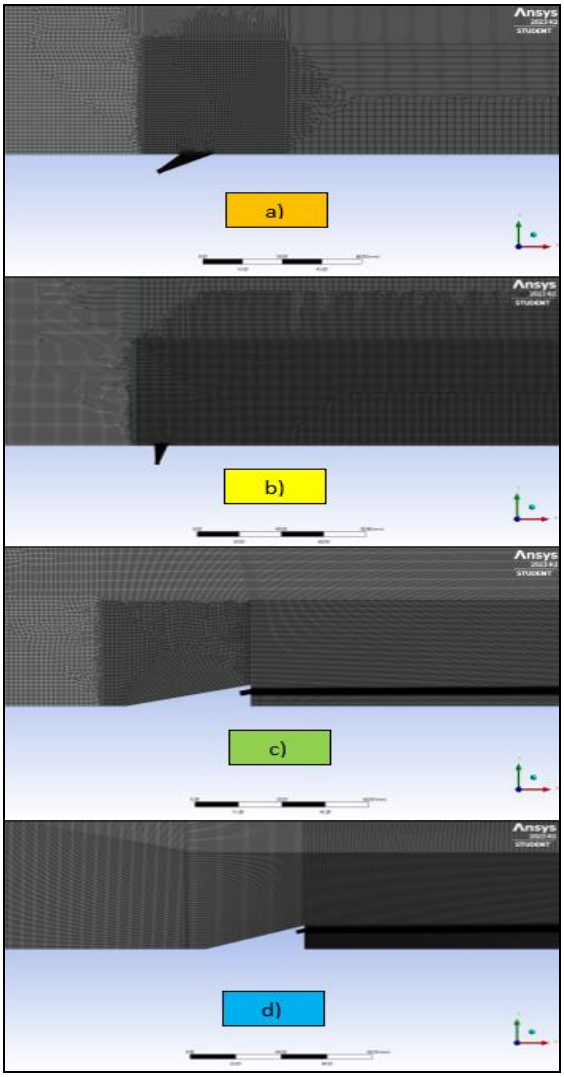

Fig 5: Mesh designs a) Mesh M1 (Case 1: 30˚ Flush wall Injector Mesh), b) Mesh M2 (Case 2: 80˚ Flush wall Injector Mesh) c) Mesh M3 (Case 3: 12˚ Ramp Injector Mesh) d) Mesh M4 (Case 4: 18˚ Ramp Injector Mesh)

Table 3: Simulation boundary conditions

Boundary Conditions			
Variable	*Air Inlet*	*Hydrogen Inlet*	*Unit*
Pressure, P	100,000	100,000	Pa
Density, rho	1.002	0.097	kg/m^3
Fluid Velocity, u	745.47	1176.86	m/s
Mach Number	2	1	-
Temperature, T	340	250	K
	Species Proportion		
N2	73.6	0	%
O2	23.2	0	%
H2O	3.2	0	%
H2	0	100	%

Table 4: Model and solver configuration

Model & Methodology			
Description	*Value*		*Unit*
	Combustor Geometry		
Combustor Height	150		mm
Combustor Length	800		mm
	Flushwall Geometry		
Inclination	30	80	°
Injector Diameter	2	2	mm
	Ramp Geometry		
Inclination	12	18	°
Injector Diameter	2	2	mm
	Setup		
Solver Type	Density-Based (Gravity Y=-9.81m/s^-2)		
Energy Equation	ON		
Turbulence Model	K-Epsilon [2 Eqn] Realizable Std. Wall		
Species	Species Transport Mixture: Hydrogen/Air Reaction: Volumetric, Eddy-Dissapation		
Materials	Fluid, Air, Viscosity: Sutherland Fluid, Air, Density: Ideal Gas Mixture, H2+Air, Viscosity: Sutherland Mixture, H2+Air, Density: Ideal Gas		

Flow velocity indicates levels of thrust that the combustor is able to produce for propulsive means, relying on the level of combustion that occurs. Static temperature is an indication of combustion efficiency of the fuel where a greater quantity of combusted fuel results in a greater static temperature. To support static temperature and flow velocity combustion observations, mass fraction contours of H_2, O_2, and H_2O can be utilised. Diminishing H_2 and O2 contours indicate the interactive diffusion of the two fluids downstream of the injector. Contours of H_2O mass fraction increasing in the combustor indicate that combustion occurs, as liquid water is indicative of a hydrogen-air combustive reaction. For *all 4 cases* examined (2 for flush wall injection and 2 for ramp injection), the contour plots are given next.

4. Ansys results and discussion

Figs. 6- 23 illustrate the contour plots for variables computed for all 4 cases simulated. For Cases 1 and 2 (flush wall) *static pressure, velocity, density and static temperature are computed. For Cases 3 and 4 (ramp injection),* these variables *and additionally mass fraction contours of H_2, O_2, and H_2O* are also provided.

4.1. Pressure contours

The primary utility of the pressure contours presented for 30˚ and 80˚ flush wall injectors in Figures 6 and 10 is to enable observation of the shockwave structures throughout the length of the combustor in each case. Alongside the contours accumulated for density, the behaviour of the flow can be analysed with respect to the compressibility effects, as elaborated in Kummitha and Pandey [13]. In the case of the 30˚ and 80˚ flush wall injectors, the point of maximum pressure occurs where the freestream air meets the injected hydrogen fuel, forming a bow shockwave due to the large difference in fluid density and velocity. Notably, in the case of the higher inclination 80˚ flushwall fuel injection, a higher maximum pressure is found to be 427kPa at the fluid interaction point due to an increased Y-velocity of the injected fuel. Meicenheimer et al. [24] also computed pressure characteristics of injectant into oncoming flow although at much lower flow velocities. Comparing our results to [21], one can confirm the validation of extreme pressure increase along the path of the injected fuel. For the 30˚ and 80˚ flushwall injectors, the highest recorded regions of pressure are very similar to those in [21] for flush wall injector behaviour. Across each shockwave there is a pressure drop of around ~40-60kPa. The flushwall injectors both feature an oblique shockwave with a wave angle of 35.7˚. Additionally, due to the initial bow shockwave formed by the injectant, a formation of 3 distinct reflected shockwave structures is computed for both cases. For the 30˚ flushwall case, in Figure 6, the layers of the first reflected shockwave are concentrated with the second to form a region that experiences a focus of pressure, at the point of shock reflection with the fuel-air mixing layer. This concentration is evident by the contour indicating that pressure reaches in excess of ~260kPa. Similarly, in the case of the 80˚ flush wall, Figure 10 indicates lower pressure concentration at the same interaction point of around ~200kPa. Increased

pressure regions are indicative of combustion due to the expansion characteristics of exothermic processes. In Figure 6 and 10, post shock mixing region interaction, a pressure increase is clearly observable in both cases. The 30˚ and 80˚ cases both experience a pressure rise of ~60kPa after the first reflected shockwave, indicating the possibility of an exothermic process.

Case 1: 30˚ Flush wall Injection

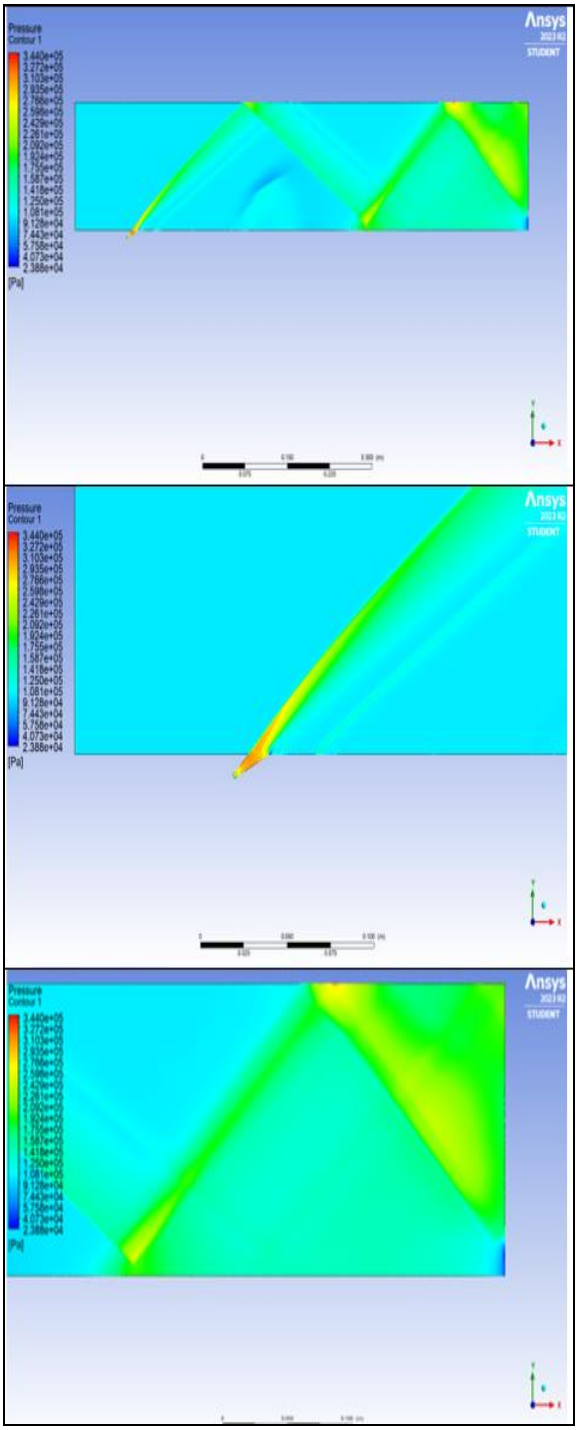

Fig 6: Static pressure contours (Case 1)
(top full plot, middle and bottom zoom shots)

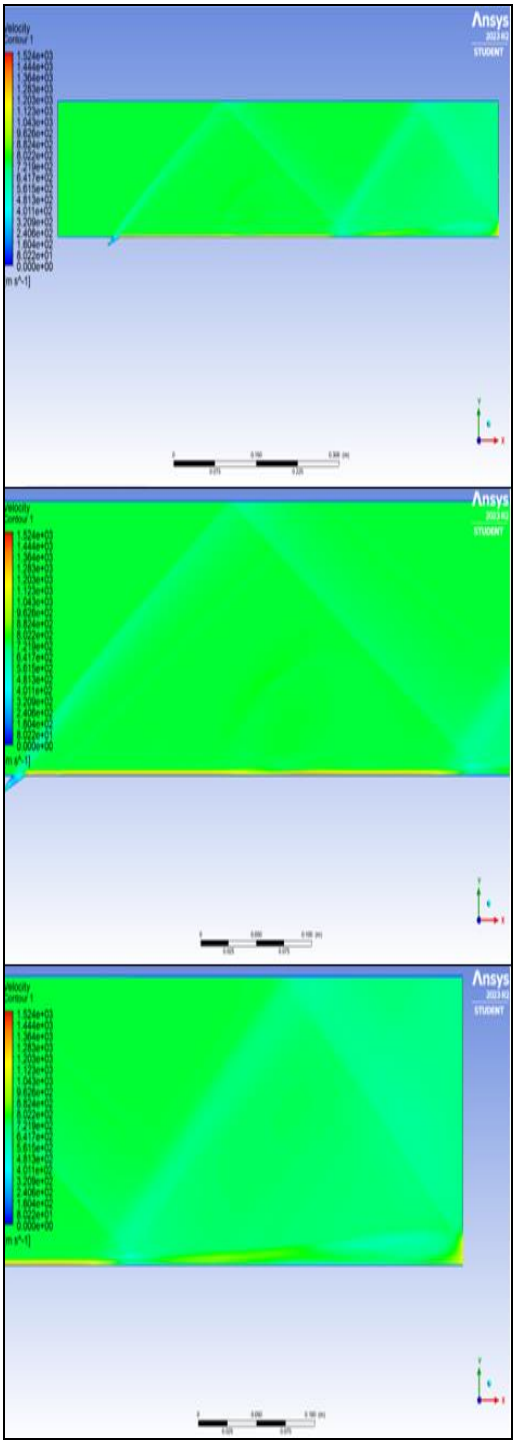

Fig 7: Velocity contours (Case 1)
(top full plot, middle and bottom zoom shots)

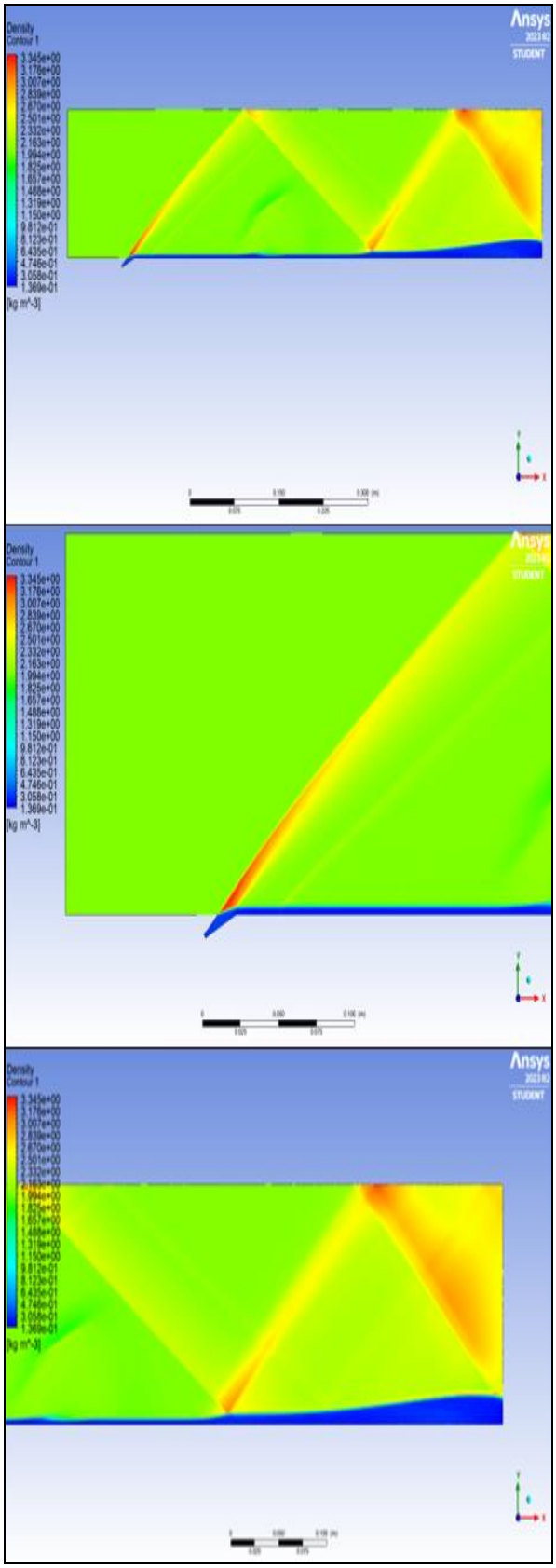

Fig 8: Density contours (Case 1)
(top full plot, middle and bottom zoom shots)

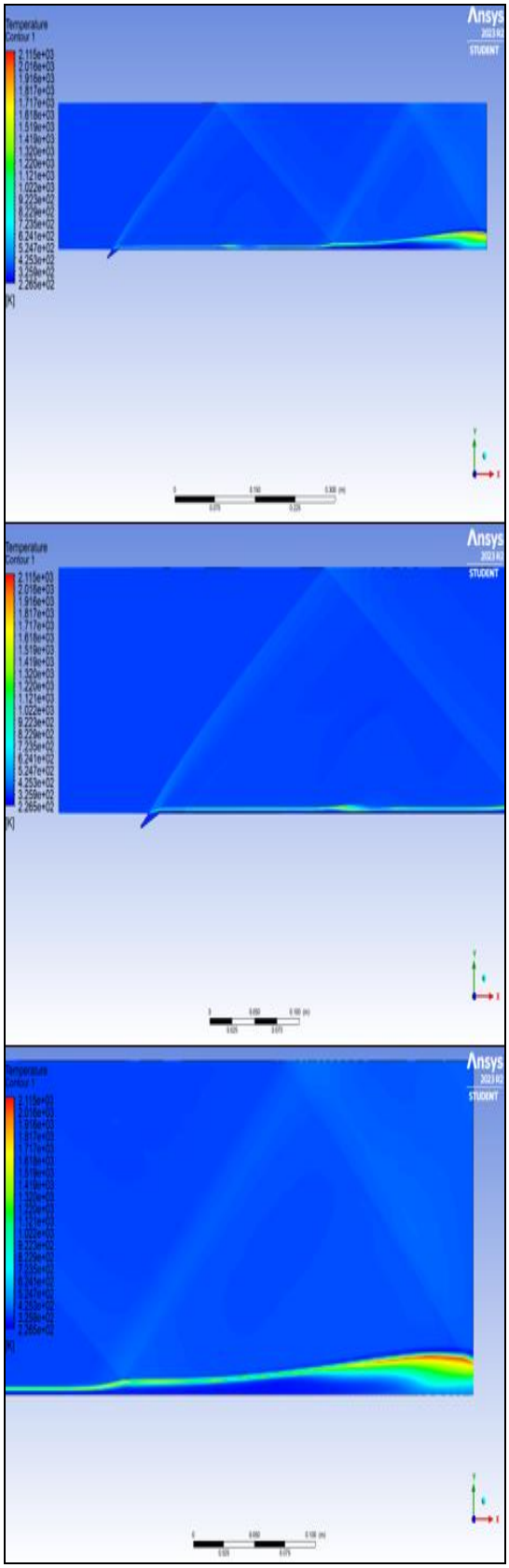

Fig 9: Static temperature contours (Case 1)
(top full plot, middle and bottom zoom shots)

Case 2: 80˚ Flushwall Injection

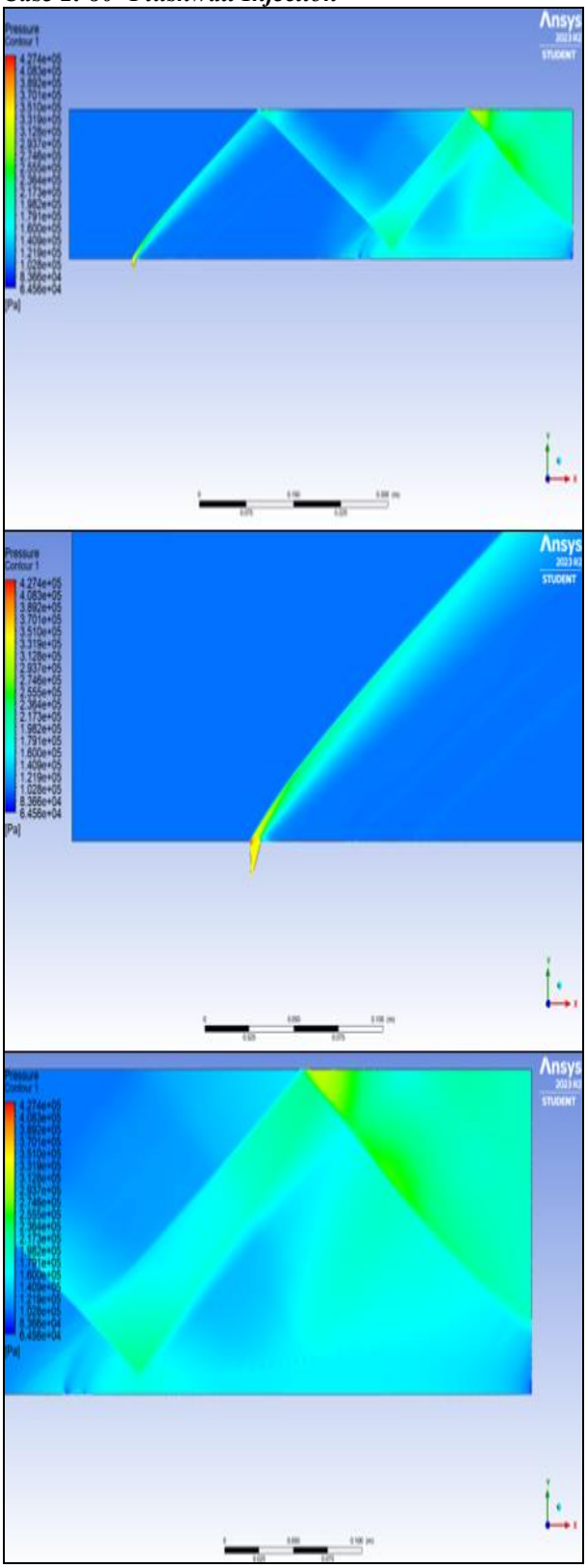

Fig 10: Static pressure contours (Case 2)
(top full plot, middle and bottom zoom shots)

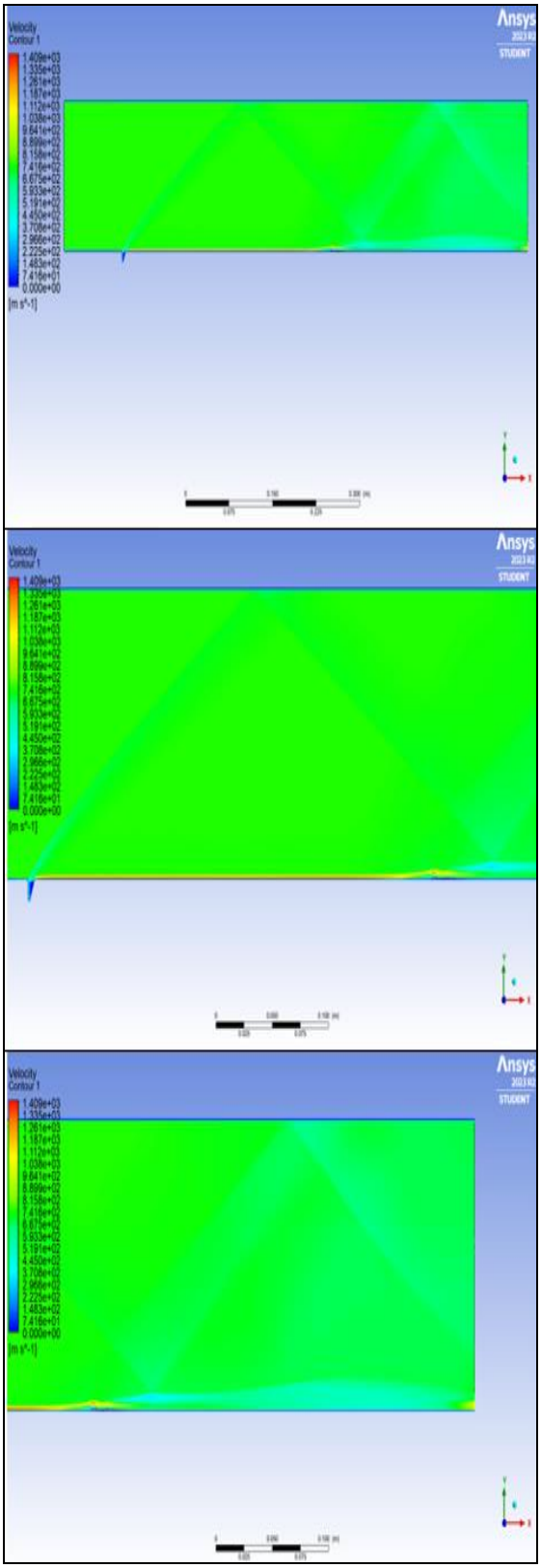

Fig 11: Velocity contours (Case 2)
(top full plot, middle and bottom zoom shots)

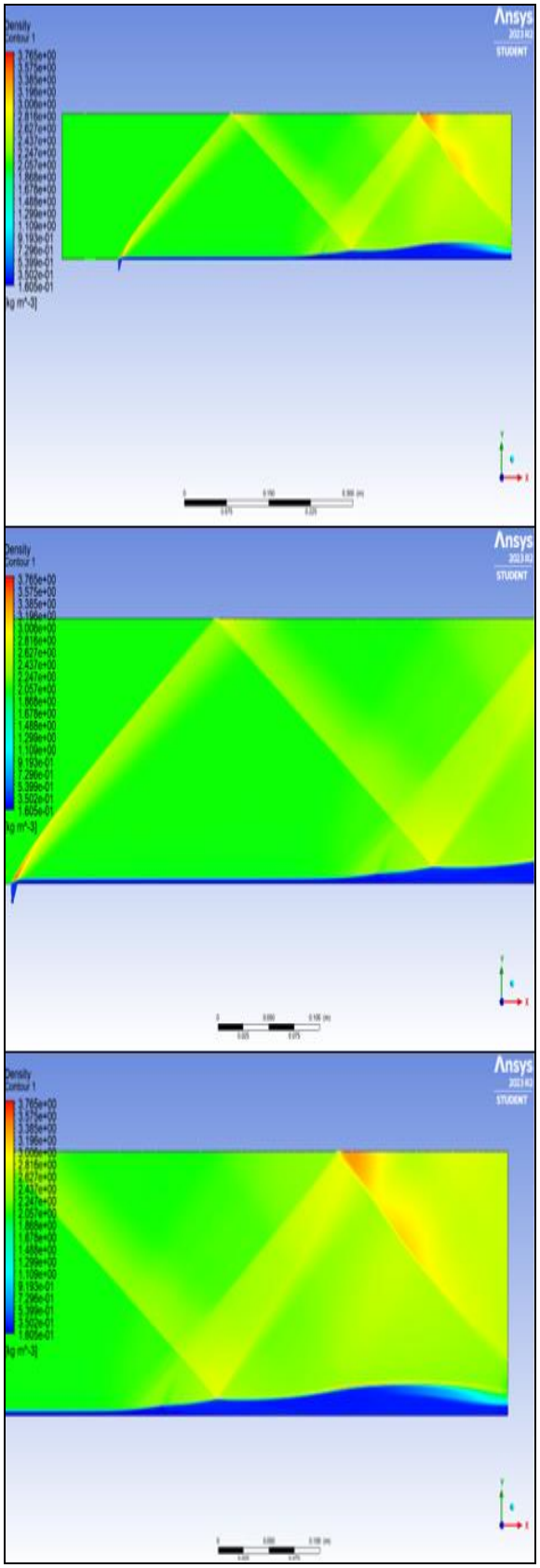

Fig 12: Density contours (Case 2)
(top full plot, middle and bottom zoom shots)

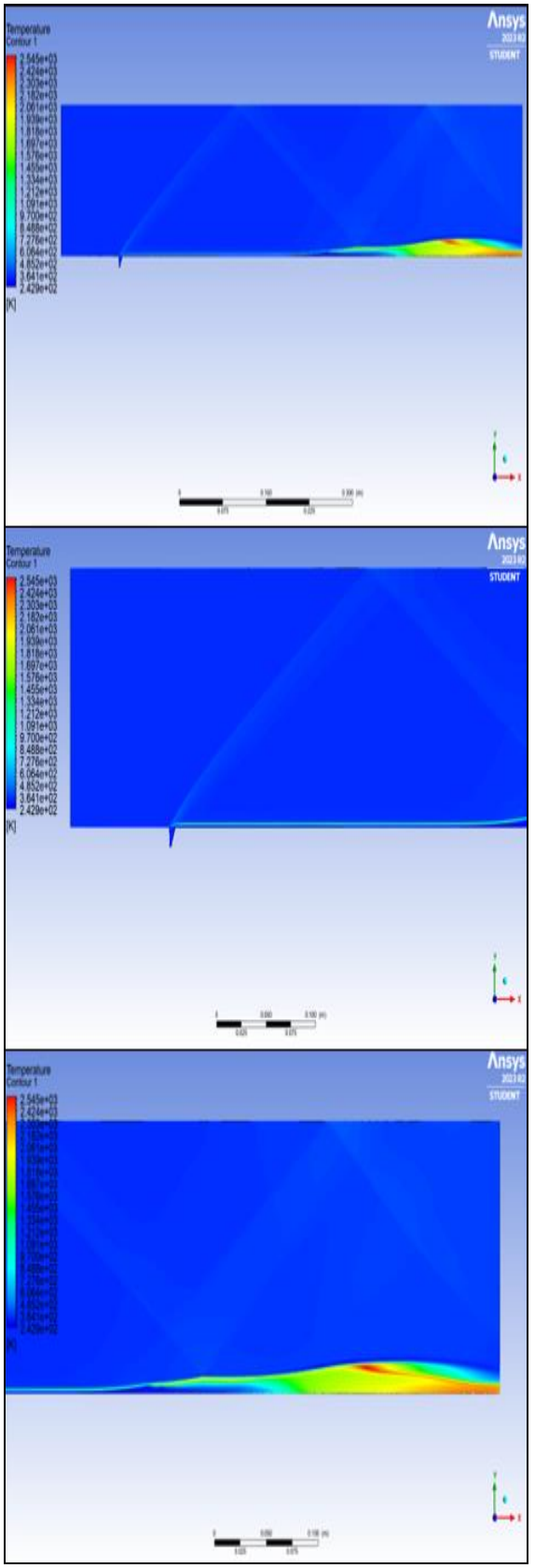

Fig 13: Static temperature contours (Case 2)
(top full plot, middle and bottom zoom shots)

Case 3: 12˚ Inclination Ramp Injection

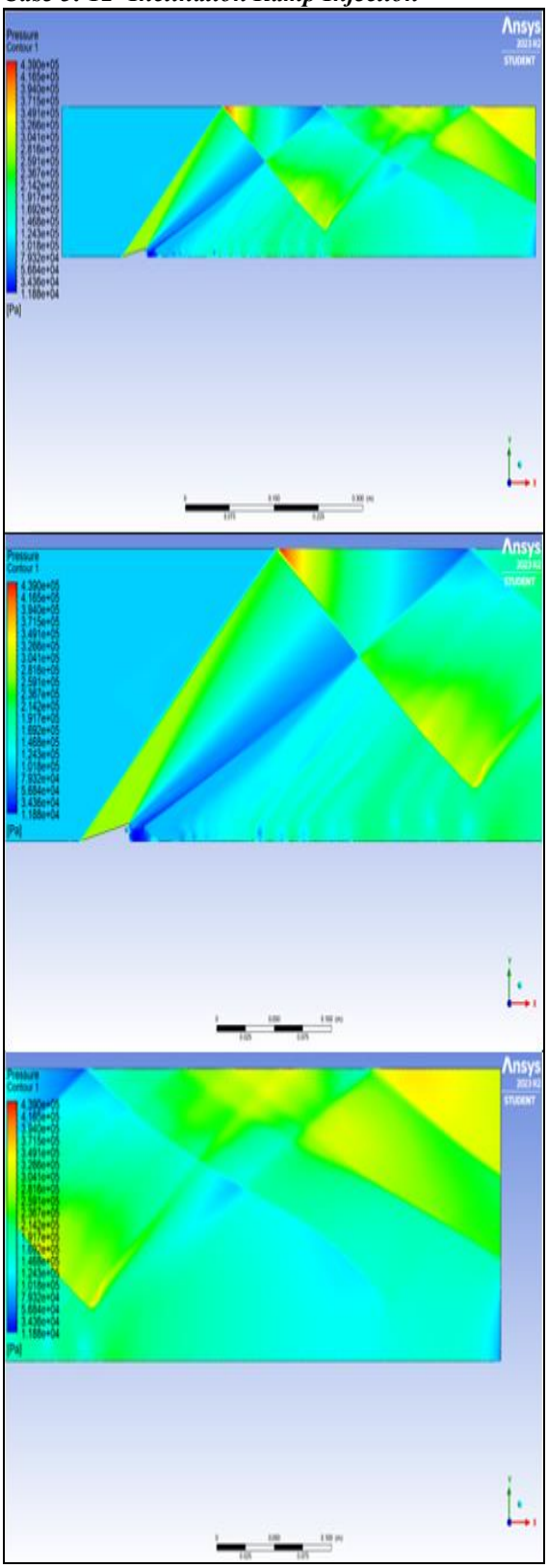

**Fig 14: Static pressure contours (Case 3)
(top full plot, middle and bottom zoom shots)**

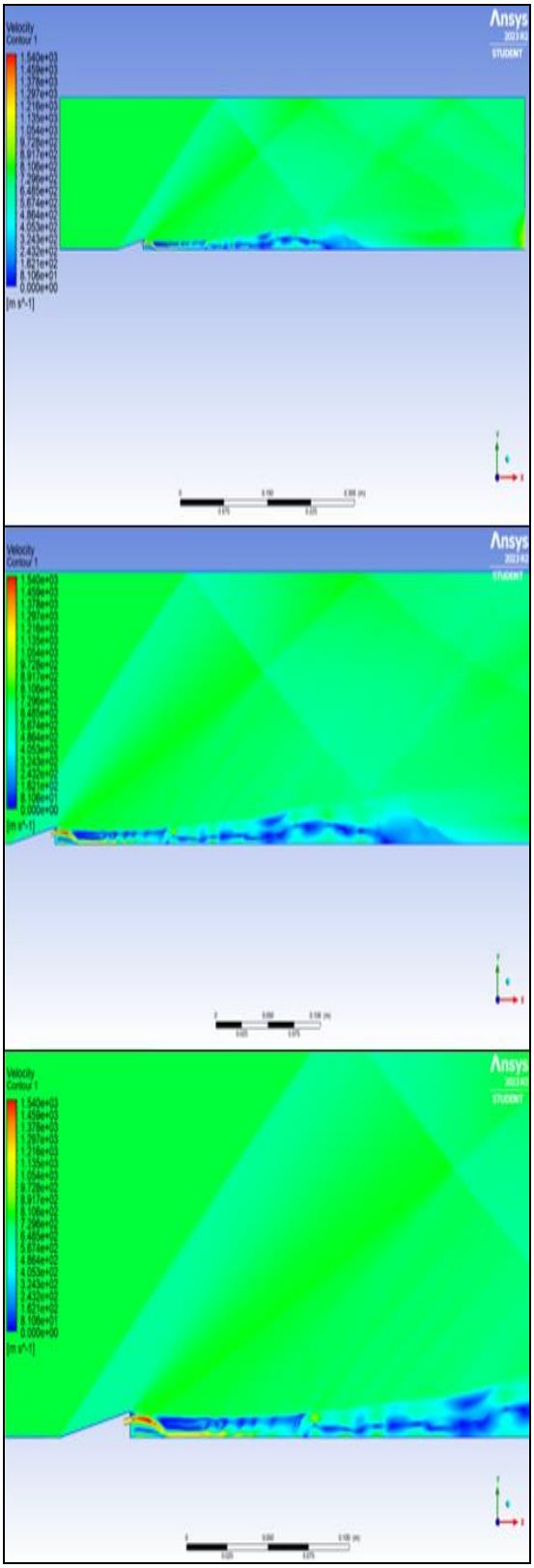

**Fig 15: Velocity contours (Case 3)
(top full plot, middle and bottom zoom shots)**

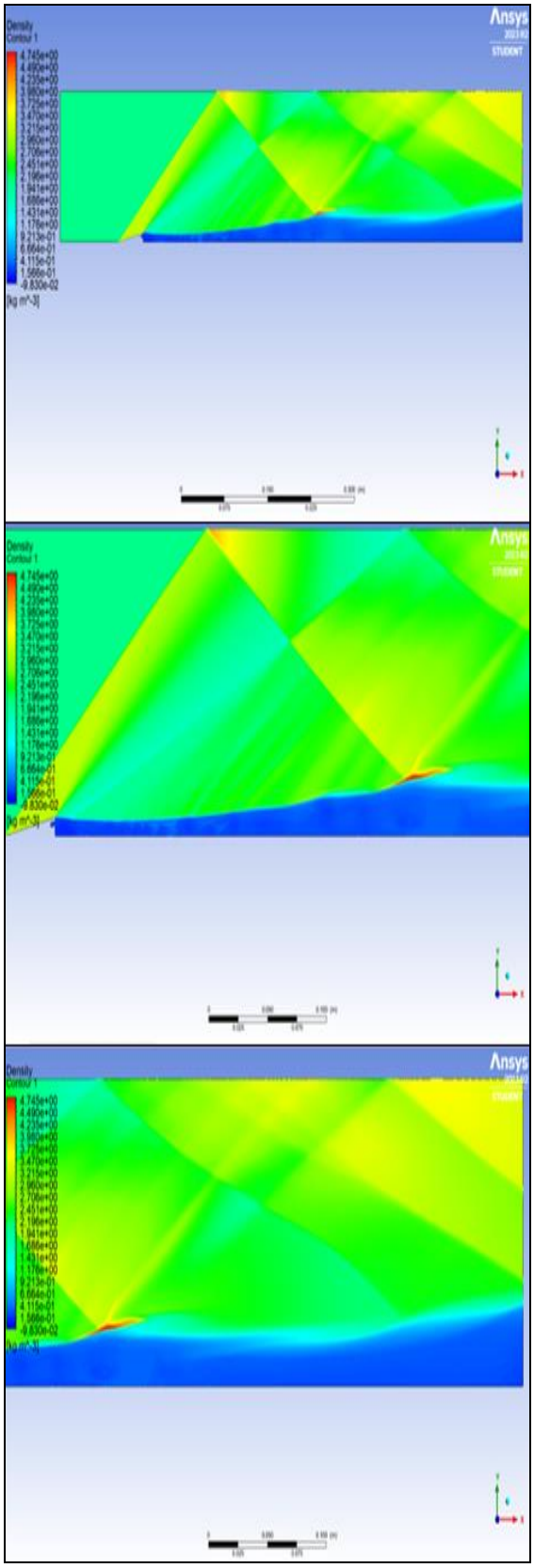

Fig 16: Density contours (Case 3)
(top full plot, middle and bottom zoom shots)

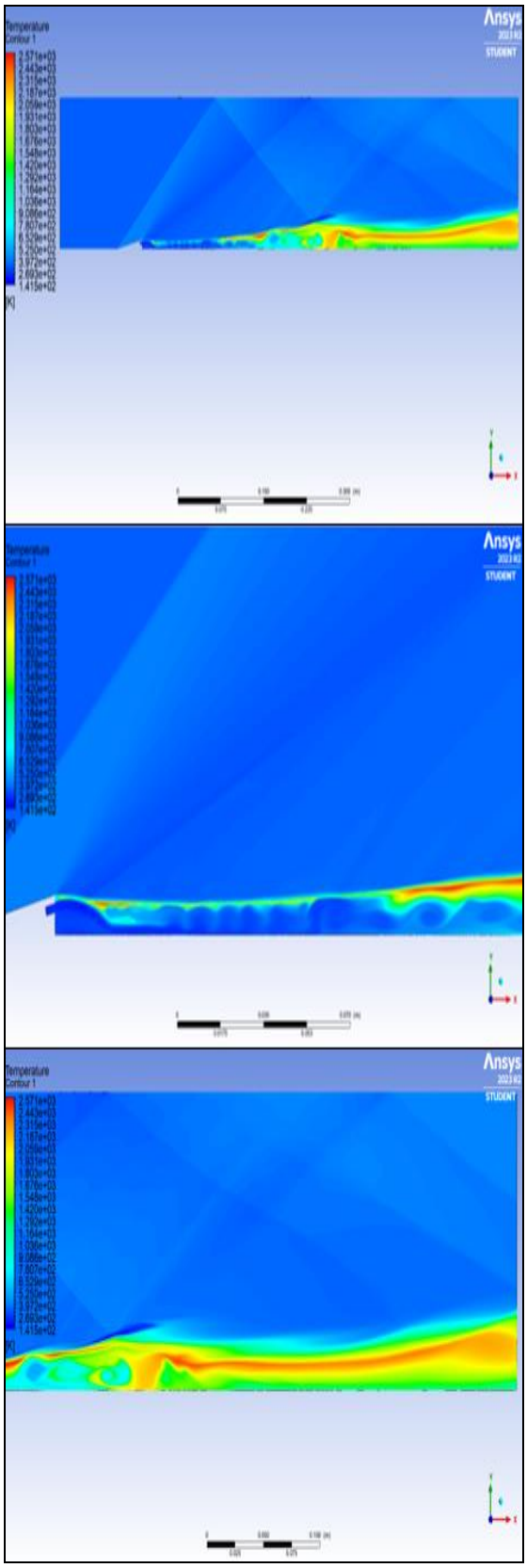

Fig 17: Static temperature contours (Case 3)
(top full plot, middle and bottom zoom shots)

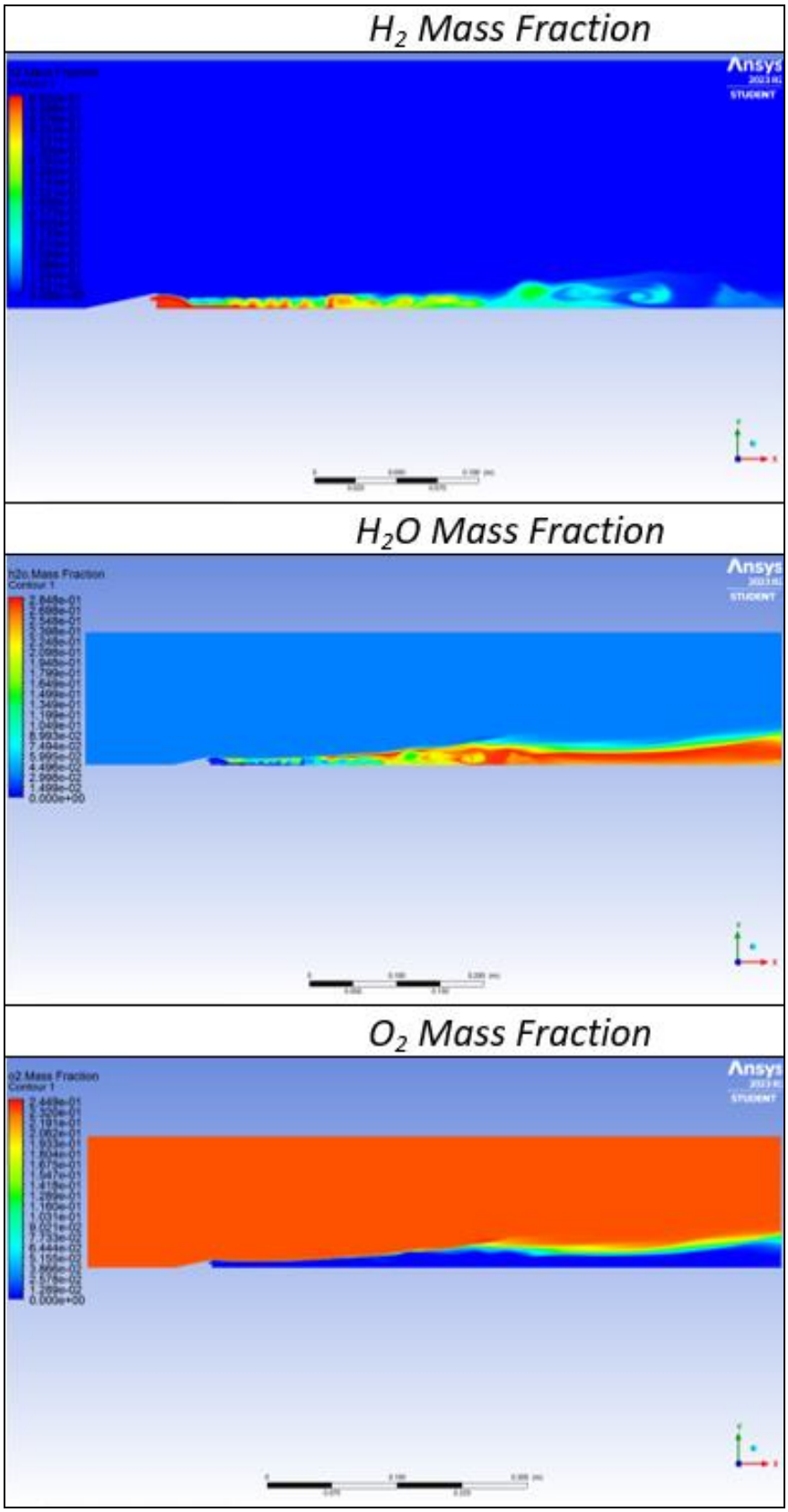

Fig 18: Computed mass fraction contours for hydrogen, water and oxygen (Case 3)

Case 4: 18˚ Inclination Ramp Injection

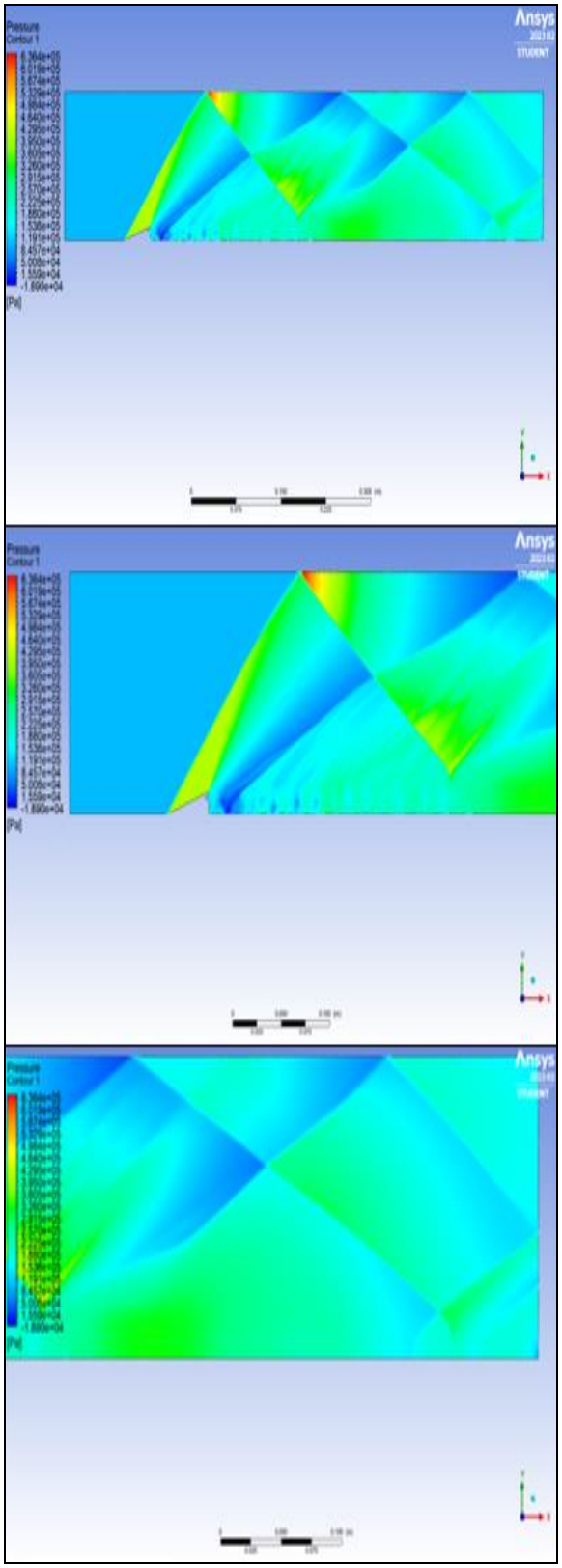

Fig 19: Static pressure contours (Case 4) (top full plot, middle and bottom zoom shots)

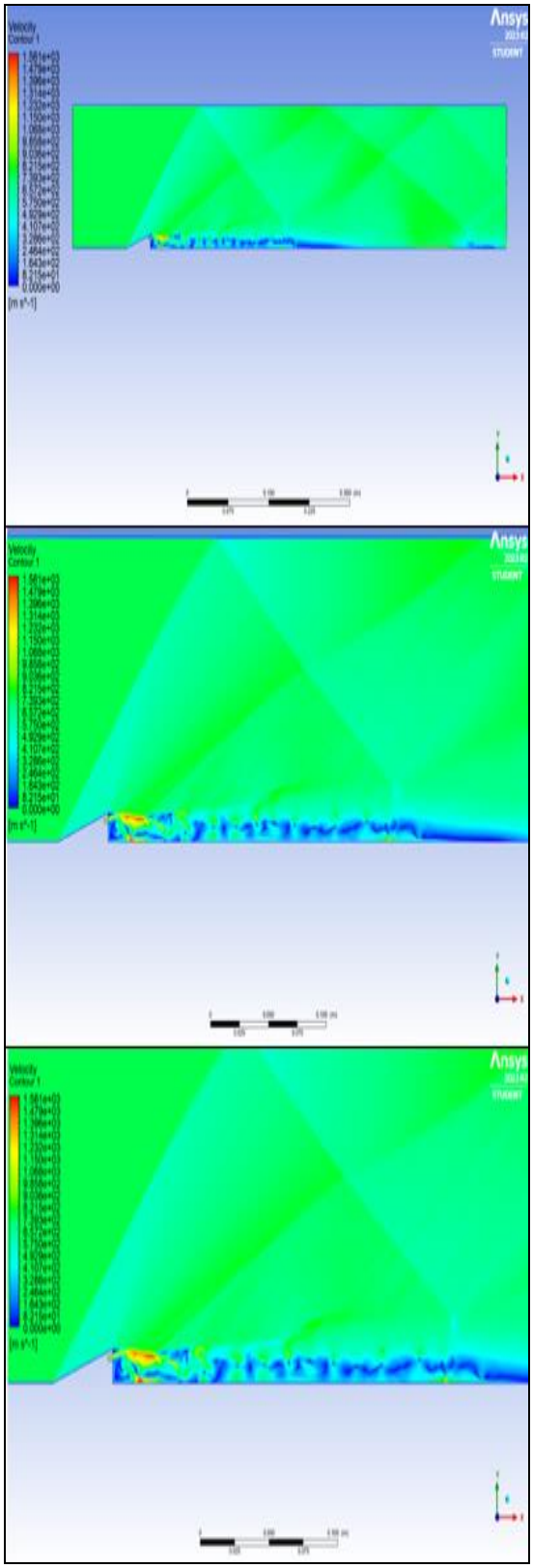

Fig 20: Velocity contours (Case 4) (top full plot, middle and bottom zoom shots)

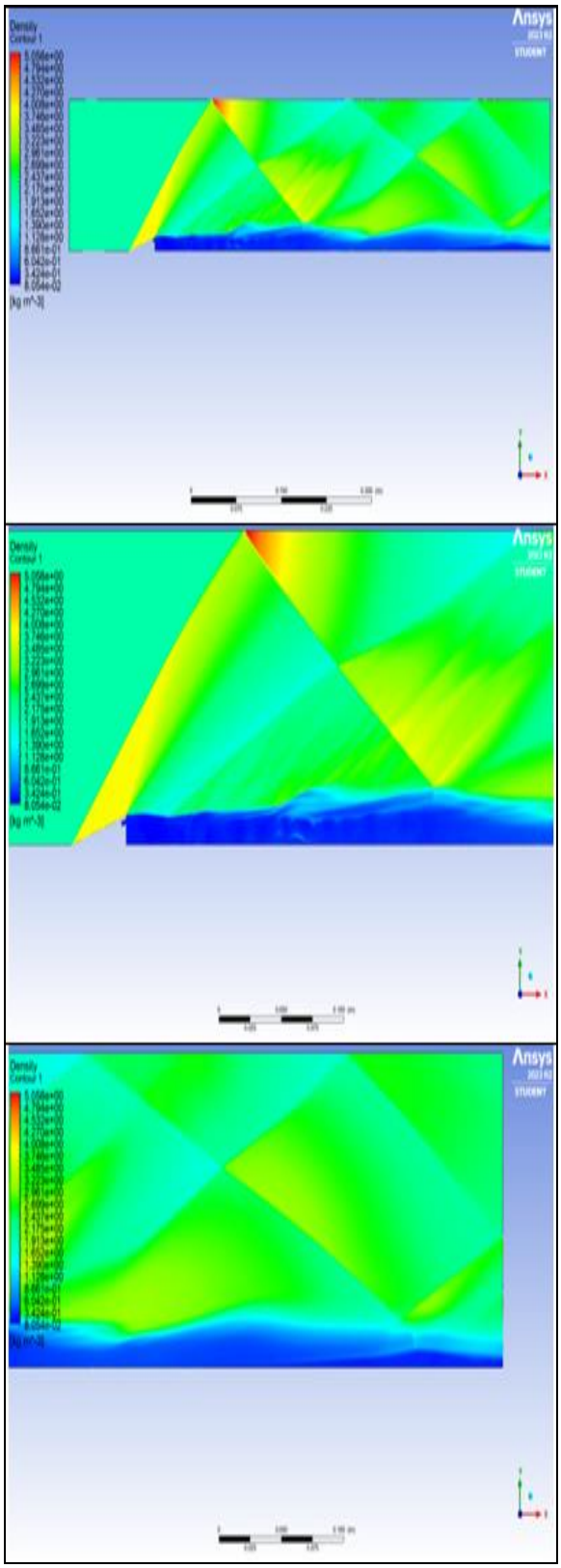

Fig 21: Density contours (Case 4)
(top full plot, middle and bottom zoom shots)

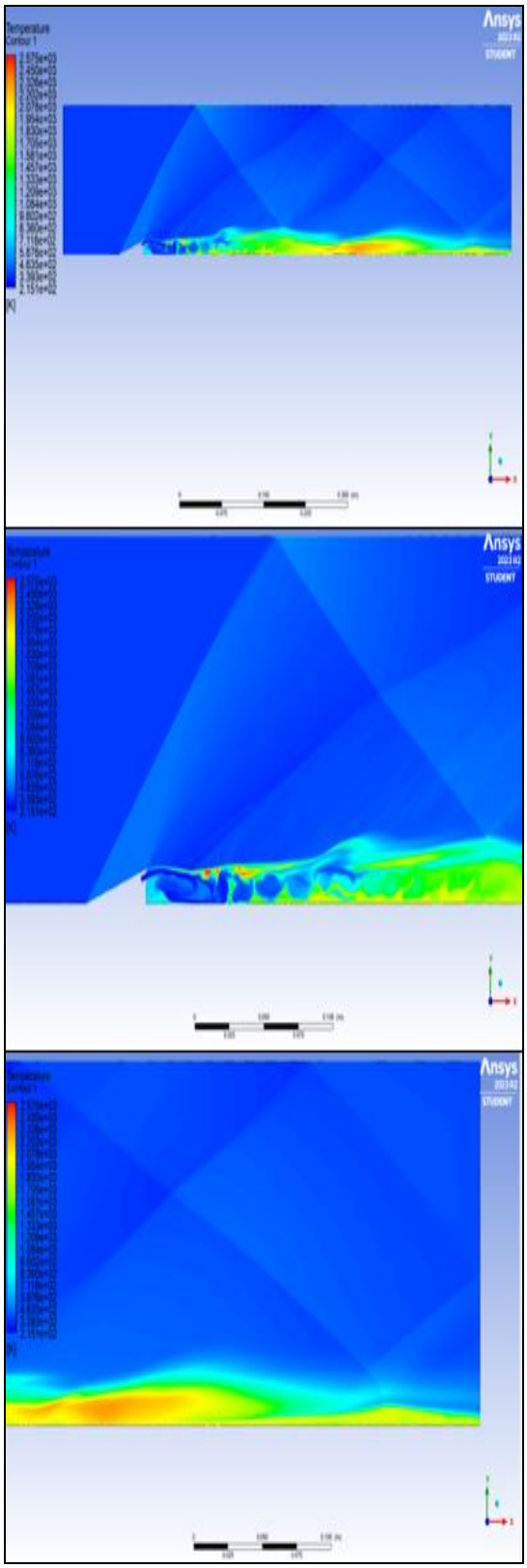

Fig 22: Static temperature contours (Case 4)
(top full plot, middle and bottom zoom shots)

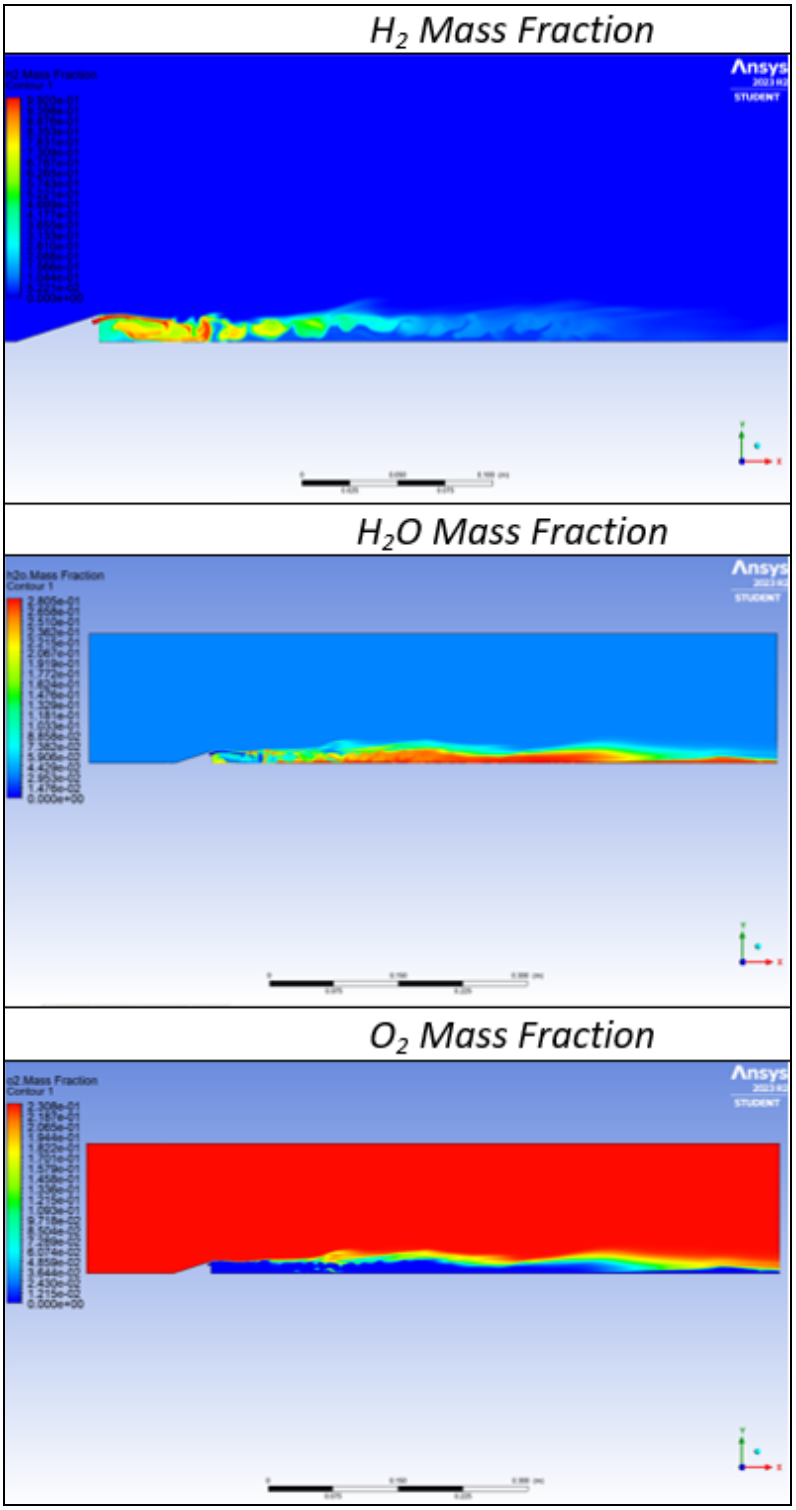

Fig 23: Computed mass fraction contours for hydrogen, water and oxygen (Case 4)

For the 12˚ and 18˚ ramp injection methods inspection of Figs. 14 and 19, given earlier, exhibit a maximum pressure between the upper wall and first reflected shockwave at pressures of 439kPa and 636kPa respectively. The combustor in the presence of the ramp injection method experiences a more complex shockwave structure downstream of injection due to the interaction of strong reflected shockwaves initiated by the forward most point of the ramp geometry, and the aft expansion fan formations. Downstream of the injector, the reflected shockwave-expansion interaction can be observed in Figure 14, whereby regions of high pressure are isolated by the interactions, forming distinct areas of high pressure called 'radical farms', explored by Odam and Paull [25]. The

presence of radical farms raises pressure and temperature which are favourable for combustion when the hotspots build to a sufficient level to release significant amounts of thermal energy. The maximum pressure in the case of the 12˚ ramp at 439kPa is significantly lower than the 18˚ ramp with a maximum pressure of 636kPa due to the intensity of the oblique shockwave required to change the direction of the flow, resulting in a greater shock angle and therefore strength. The radical farms presented by Odam and Paull [25] correlate closely with the ANSYS FLUENT results in Fig. 14 and 19 for both the 12˚ and 18˚ ramp injector cases. These regions in the present design cases are a result of basic geometry and not full specification and represent a configurable addition to the combustor geometry to isolate and focus ignition to a particular region.

4.2. Velocity Contours

The velocity contours presented for flush wall injection at 30˚ and 80˚ inclination in Figures 7 and 11 suggest small velocity potential along the combustor. In both flush wall injection cases, the regions of highest flow velocity occur along the boundary layer of the wall surface where fuel is introduced. In the case of the 30˚ flush wall injector, a maximum velocity of 1,500m/s is reached immediately downstream of fuel injection where the oncoming Mach 2 airflow exerts shear force on the introduced fuel, accelerating it to the velocity produced. In the case of the 80˚ flush wall injector, similar behaviour is observed whereby the maximum flow velocity is 1,409m/s immediately downstream of injection where the Mach 2 airflow meets the flow of fuel into the combustor. The 30˚ injector experiences a higher maximum velocity, which is due to the x-component velocity of the flow being higher for the 30˚ injection, resulting in a lower cumulative velocity in the case of the 90˚ injector, with a smaller x-component. The 30˚ and 80˚ Flush wall injectors produce minimum mixing which limits their production of thrust and ultimately velocity potential. In both cases, the velocity is reduced dramatically upon the fuel and air mixing layer interaction with the reflected bow shockwave. For the 30˚ flush wall injector in Figure 7, the velocity recovers to around 800m/s, but in the case of the 80˚ flush wall injector (Figure 11), reduces to around 370m/s after the reflected shockwave interaction, indicating an inadequate level of combustion takes place for sufficient production of thrust. The 80˚ flush wall injector suffers a much higher reduction in velocity after the shockwave interaction and is likely due to the turbulence that appears at around 500mm of the combustor length, which develops after the shockwave and results in recirculation and vortices, further reducing the velocity of the flow. Earlier studies e.g. Drozda et al. [4] noted that the key performance influencing design parameter for flush wall injection is combustor height. Unsurprisingly, the velocity contours in Figures 7 and 11 for the 30˚ and 80˚ cases reflect the minimal distribution of velocity toward the centre stream of the combustor suggested by the study. The cross-stream contours emphasise the minimal infiltration characteristics of fuel injectant i.e. hydrogen, where the height of the duct is equal to the height of the combustor. By this measure, the contours for the present case illustrate penetration height to be no greater than the height of the injector.

The 12˚ and 18˚ ramp injection methods presented in Figures 24 and 25 (which have been annotated based on the earlier Figs. 15, 20) respectively, feature significant velocity fluctuations, suggesting good mixing levels which favour effective combustion. The 12˚ ramp (Figure 24) experiences a maximum velocity of 1,540m/s at the point of fuel injection and a stretched recirculating fuel-air mixing zone up until the point of suggested combustion. The highly vortical recirculate zones are suggested in Figure 24 where the rotational momentum of the flow causes the effective velocity of the flow to tend toward 0m/s. In the case of the 18˚ ramp, the maximum velocity is 1,561m/s and similar to the 12˚ ramp, features an elongated fuel-air recirculation zone where the velocity tends toward 0m/s. Comparatively, the 12˚ ramp has a recirculation zone of greater length and intensity than the 18˚ ramp, with the vortical effects protruding much more into the oncoming air layer. The enhanced mixing and recirculation experienced by the 12˚ ramp combustor case is likely due to the reduced strength of the reflected oblique shockwave. The 18˚ ramp experiences a high strength oblique shockwave as observed in Figure 25, resulting in greater pressure loss at the point of the fuel-air mixing layer when the shock is reflected. The influence of this reflected shock is reduced in the case of the 12˚ ramp to allow for extensive mixing of the flow. At the suggested location of combustion occurrence presented in Figures 24 and 25, after the reflected shock interaction, it is observed that the velocity in both cases recovers to around 860m/s. Coinciding with the 12˚ and 18˚ ramp pressure contours presented in Figures 24 and 25 respectively, a drop in pressure can be observed with an increase in velocity, exhibiting behaviour in line with Bernoulli's principle. In both cases the flow behaviour of recirculating regions immediately downstream of the ramp injector aft surface is captured. As the oncoming freestream flow passes over the ramp boundary layer, momentum transfer takes place in the form of an imparted tangential velocity and friction, causing rotational flow and subsequent vortices. The behaviour can be observed where the velocity magnitude arrows tend to 0. For both Figs. 24 and 25, the computed ramp velocity contours indicate the elongated recirculation zones where velocity tends to 0.

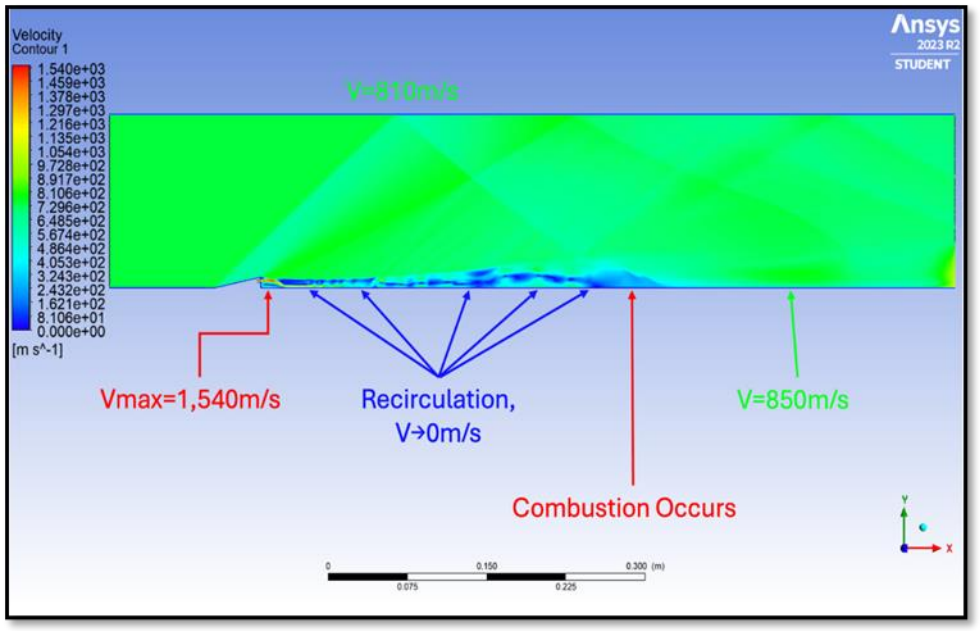

Fig 24: Annotated 12˚ Ramp Velocity Contours

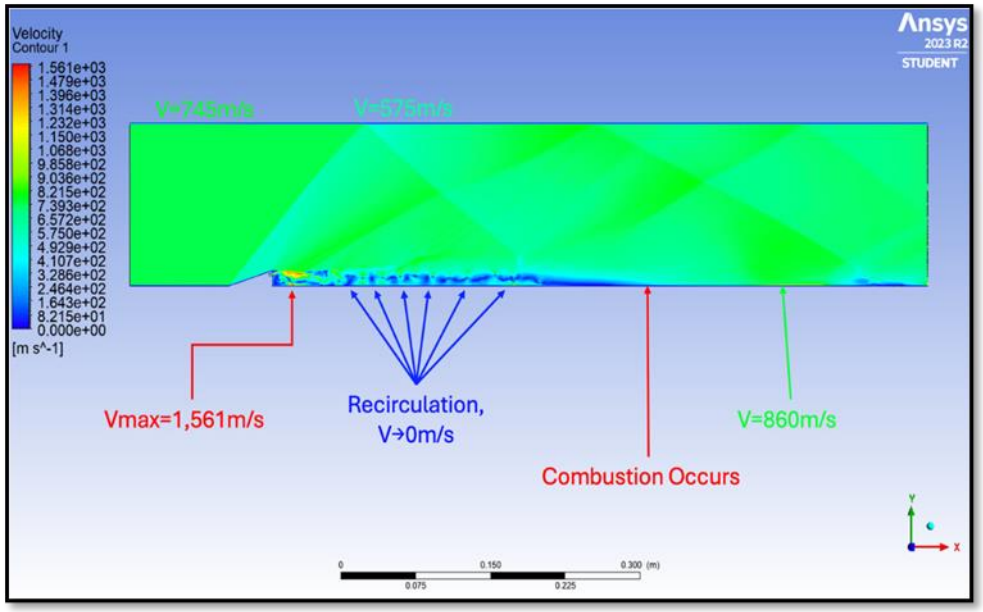

Fig 25: Annotated 18˚ Ramp Velocity Contours

4.3. Density Contours

The density contours displayed in Figures 8, 12 (flush wall injection cases of 30 and 80 degrees) and also Figures 16, 21 (ramped injection cases of 12 and 18 degrees) indicate the presence and interactions of shockwaves, in addition to initial air-fuel mixing. The shockwave behaviour presented by the density contours are identical. However, due to the distinct fluid densities, additional shock interaction behaviour can be identified. Due to the extreme low density of hydrogen fuel relative to the oncoming Mach 2 airflow, the distribution of the fuel and air are distinguishable. Inspection of Figures 8, 12 indicates that the 30˚ and 80˚ flush wall injectors introduce fuel primarily into the boundary layer, with minimum enhancements to mixing and the probability of consistent combustion for sufficient thrust production. Comparatively, observing Figures 16, 20, it is evident that the presence of the ramp geometric shape modifies density distribution more effectively and promotes good mixing by introducing significant levels of turbulence and vortices to the flow. In both flush wall cases (Figs. 8, 12), a recirculation bubble upstream of the reflected shockwave interaction is observable and responsible for enhanced downstream mixing characteristics. The 30˚ and 80˚ flush wall density contours emphasize the shock structures and

importance of utilising them as a potential design condition. The top of the fuel layer in the case of the 12˚ and 18˚ ramps indicates good mixing, suggested by the lighter streamwise contours at the fuel-air interaction layer. Higher densities along this layer represented as a transitional blue contour indicate good mixing as the low density of the hydrogen fuel and higher density of the air mix to form a combustible mixture. This mixing behaviour is minimal with the flushwall injection method due to the fuel being introduced directly into the boundary layer. Observing Figures 16 and 20, the ramp injection method distinctly promote mixing, visible in the 12˚ and 18˚ ramp cases downstream where the mixing layer fluid density is 1.300kg/m^3 and 1.652kg/m^3 respectively. The enhanced mixing characteristics presented by the ramp injection method is due to recirculation zones occurring immediately downstream of fuel injection due to the introduction of fuel at a higher intrusion point in the flow, as observed with cavity flame-holding injection methods, and noted by Liu et al. [26] and Ben-Yakar and Hanson [27]. In all simulated cases there is a distinct enhancement of fuel diffusion with the supersonic air at the point where a shockwave reflects from the low-density fuel layer. In the case of the 30˚ and 80˚ flushwall injectors, the shock-induced mixing is highly favourable due to the lack of fuel diffusion prior to the shockwave interaction, observable in Figures 16 and 20. A ramp injection case subject to Schlieren image type flow analysis by Kouchi et al. [28] highlights the observed shockwave behaviour for ramped injection. Notably, the Schlieren images emphasise the presence of reflected ramp leading edge shockwaves and the interaction with the fuel-air mixing layer. Recompression shocks and shock-induced mixing and combustion effects are also highlighted by [28], where the regions bounded by reflected and recompression shocks illustrate the formation of radical farms along the combustor length.

4.4. Temperature Contours

Figs 9, 13 show the static temperature contours for Cases 1 and 2 (flush wall injection cases of 30 and 80 degrees) and Figures 17, 21 display the static temperatures for Cases 3 and 4 (ramped injection cases of 12 and 18 degrees). Critically, the temperature contours assist in visualisation of regions with high temperatures that are a key indication of combustion. Typically, higher temperatures achieved due to combustion result in increased fluid velocity. The expansion of heated gases as a result of heightened local kinetic energy are responsible for the characteristic velocity increase. Additionally, increased temperature gradients result in enhanced mixing and therefore potential higher rates of combustion due to volatile velocity distributions induced by turbulence in the flow. In the case of the 30˚ flush wall injector (Fig. 9), a maximum temperature achieved in the combustor of 2,115K arises at the combustor exit. Elevated temperatures are recorded at the fuel-air mixing layer along the boundary layer indicating mixing and heat transfer is taking place due to viscous friction. Despite the elevated temperatures, minimum mixing characteristics are observable as suggested by the earlier density and velocity plots for the same injectors. The absence of good diffusion results in no effective combustion taking place across an effective cross-sectional area of the combustor. At the reflection point of the bow shockwave, shock-induced combustion effects are observed in the form of enhanced mixing and heat transfer. When the shockwave reflects from the fuel-air mixing layer, the layer is observed to be elevated or spread among a greater cross-sectional area, in addition to a transfer of shock energy in the form of heat, to raise the fuel-air mixing layer to a temperature of ~1,600K at the point of reflection. Due to the enhanced mixing and heat experienced after the reflected shockwave, downstream it is evident that greater recirculation is induced, and combustion occurs. Furthermore, the corresponding pressure contour given earlier suggests an elevated gas pressure which is expected in the case of combustion. Similarly, in the case of the 80˚ flush wall injector, the deficiency of sufficient turbulent flow characteristics results in delayed combustion. As in Figure 13, for the 80˚ flush wall injector a maximum temperature was recorded of 2,545K, indicating effective mixing and detonation of present fuels. Adversely, similar to the 30˚ flush wall injector, the 80˚ case experiences delayed combustion likely attributable to the shock-induced combustion phenomenon. As the shock reflects, a thin layer of the fuel-air mixing region is raised to a temperature of ~2,060K. In combination with enhanced turbulent effects due to velocity instabilities introduced by the shockwave; leads to a larger and more intense region of combustion with the maximum observable temperature of 2,545K. Comparatively, the 80˚ flush wall injector experiences higher temperatures over a wider cross-sectional area due to greater mixing levels due to an increased shockwave strength as a result of the 80˚ flush wall injector having a greater y-velocity of injected fuel. In both flush wall injector cases, delayed combustion is observed which is attributable to enhanced mixing and induced combustion associated with the reflected shockwaves.

The temperature contour of the 12˚ ramp injector as presented in Figure 17 indicates extensive mixing heat-transfer characteristics and good levels of combustion. The 12˚ case experienced a maximum temperature of 2,545K within a reasonable distance from fuel injection and pre-shock, illustrating initially that the ramp injection type is more effective at achieving combustion quickly, without the requirement for shock-induced combustion. Recirculating flow effects are directly observable primarily in the corresponding velocity contour in Figure 15, which favours good combustion downstream. As reflected in the density contour presented earlier in Figure 16, a relatively large cross-sectional area of the combustor is occupied by the fuel-air mixing layer and later by

combustive regions. The temperature contour for the 12˚ ramp injection type displays rapid diminishing of the initial H2 temperature of 250K. Downstream regions of raised temperature are likely caused by turbulent recirculation effects introducing heat into the lower regions of the fuel-air mixing layer from the top layer of combustion where the maximum temperature is recorded. Furthermore, enhanced mixing and combustion is observable after the interaction of the fuel-air mixing layers and the reflected oblique shockwave where turbulent effects are enhanced, promoting mixing, and creating a mechanism for sustained and consistent combustion throughout the length of the combustor. Enhanced mixing is observable in the associated Figure 16 where the density contour illustrates an expansion of the fuel-air mixture at the modelled exit of the combustor. This further indicates that combustive effects take place at the point of maximum temperature and are associated with a steadily increasing gas pressure. The case of the 18˚ ramp injector (Figure 21) exhibits similar characteristics to the 12˚ case, but with diminished combustive stability and effective expansion. The maximum temperature of 2,545K is experienced for both the 12˚ and 18˚ ramp cases, however the 18˚ case experiences this temperature closer to the point of fuel injection. Due to the elevated and more intrusive platform of the 18˚ ramp, a downstream region of greater turbulent intensity can be observed, evident in both the density contour in Figure 20 and in the significant recirculation zones between the fuel injection and shock interaction point. The 18˚ temperature contour indicates that the diffusion of thermal energy is sufficient with mid-mixture-streams reaching a temperature of around 1,450K, increasing to a maximum of ~2,360K post shock interaction and quickly diminishing temperature thereafter. However, the 18˚ ramp produces undesirable, inefficient fuel-air mixing prior to the reflected shock interaction. The intensity of the reflected shockwave in the case of the 18˚ ramp would be stronger, imparting more energy upon the fuel-air mixing layer. Presumably, the diminished temperature distribution of the 18˚ case against the 12˚ case is a result of ineffective mixing and the mixture being unable to fully benefit from downstream shock-induced combustion effects. Due to the greater oblique angle of the 18˚ ramp, the reflected shock and fuel-air mixture interaction is witnessed much closer to the injector, where insufficient mixing has been able to occur. This produces sub-optimal mixing and reduces combustion efficiency of the scramjet.

4.5. Combustion mass fraction contours

Figs 18 and 23 visualize the mass fraction contours for hydrogen, water and oxygen for Case 3 (12 degrees ramp inclination) and Case 4 (18 degrees ramp inclination). H2O mass fraction of the 12˚ ramp in Figure 18 can be utilised to evaluate the extent of the combustion across the cross-sectional area. H2O, or water vapour is a primary by-product of combustion and is directly indicative of combustion occurrence. It is apparent that the H2O mass fraction for the 12˚ ramp injector indicates immediate, minor, unstarting regions of combustion as confirmed by high intensity areas of water vapour along the top of the fuel-air mixing layer. The generation of H2O is intensified with greater downstream distance and after the reflected oblique shock interaction, the recirculation of the mixing region is seen to become more stable. The uniform and even distribution of combustion by-products in the form of water vapour therefore indicates stable and useful combustion for the production of thrust. Additionally, toward the modelled exit of the combustor, the combustive region appears to be expanding into more of the cross-sectional area. The associated pressure as observed in Figure 14 increases as combustion takes place as expected and drops as the combustion becomes uniform and accelerates the flow up to around 860m/s. Figure 23 suggests the distribution of the combustion by-products in the form of water vapour as presented for the 18˚ ramp case. The contour suggests that the 18˚ case experiences more frequent and isolated regions of combustion closer to the injector. Additionally, combustion can be observed in the top layer of the fuel-air mixture as well as near the boundary layer, due to the heightened recirculation as a result of an elevated injection platform introducing greater turbulence into the flow. Greater temperatures at the boundary layer are responsible for the development of combustion closer to the lower wall where good levels of combustion are suggested by the presence of H2O along the combustor. Comparatively, the 12˚ and 18˚ cases achieve the same maximum temperature, and extensive regions of stable combustion along the combustor length. However, the 18˚ case, while experiencing a combustive region of comparable temperature and combustion much closer to the injector, features a combustive region that cools and diminishes exhibiting an opposite trend to the 12˚ case, where the region contracts by the exit of the combustor. In both ramp injection case, similar oxygen mass fraction and hydrogen mass fraction distributions are also observed, although for the 12 degrees case (Fig. 18) greater magnitudes of hydrogen mass fraction are computed for a more protracted region along the longitudinal direction in the upstream. This correlates with the more intense combustion produced for the 12 degrees case. Oxygen mass fractions are generally larger for the 18 degrees case, however. In ramped injectors exothermic reactions are observed in the form of combustion with resultant H2O products. The ANSYS computations capture the expansive behaviour and consistent temperature distribution throughout the length of the combustor for both 12˚and 18˚ cases. However, since the current simulations are confined to 2-dimensional analysis, the present study lacks the 3-dimensional effects arising in actual scramjets, and this constitutes a very good pathway for future studies which may also encompass simulating the immediate reaction process in combination

with excessive turbulent effects induced by the ramp geometry.

5. Conclusions

A theoretical and numerical study of ramp injection and flush wall injection effects in 2-dimensional supersonic combustion in a scramjet has been presented. The flush wall injection method (with 30 degrees and 80 degrees designs) was analysed in the present study to further explore flow characteristics despite the appeal of high-pressure recovery for combustion. By similar measure, the ramp injection method (with 12 degrees and 18 degrees inclinations) was presented for study to circumvent low pressure recovery encountered by strut injection methods, where mixing is optimal but the potential for effective combustion is reduced. The RANS model and ANSYS FLUENT density-based solver was deployed and numerical results generated for static pressure, temperature, velocity, density and hydrogen/water/oxygen mass fraction contours. Detailed mesh designs were presented using quadrilateral elements. The material properties of air and the mixture (hydrogen-air) feature ideal-gas density and Sutherland's viscosity for heat transfer properties to accurately simulate compressibility effects. A two equation, realizable k-epsilon turbulence model is employed with standard wall treatment, to encompass superior simulated rotational spreading behaviour of the flow. To model the mixing, heat transfer, and combustion with the realizable k-epsilon model, a volumetric, hydrogen-air mixture Species-Transport model with Eddy-Dissipation turbulence-chemistry interactions was deployed with turbulent Schmidt number of 0.7 and a turbulent Dissipation Rate (TDR) of 1.2. Two distinct fuel injection methods are presented in this study- the transverse flush wall injection and the ramp method. The hydrogen fuel is injected through a port with a 2mm cross-sectional area. The main findings of the computations can be summarized as follows:

(i) The simulative results obtained feature a complex series of shockwave structures in all 4 cases.

(ii) The primary distinction between flush wall and ramp injection structures observed due to compressibility effects is the additional effect of radical farming along the combustor length in the case of ramp injectors, due to oblique shockwaves and expansion fans induced by the intrusive ramp geometry.

(iii) The "radical farms" observable in pressure and density plots for the ramp injection provide a foundation for the potential focusing of thermal and pressure characteristics in aid of combustion.

(iv) The shockwave structures in the case of flush wall injectors are fairly simple with only reflected oblique shockwaves to serve as additional mixing enhancement.

(v) The density and pressure contours overall are useful for observation of shock-induced mixing and combustion behaviours, critically in the case of the flush wall injectors for any useful mixing and combustion the simple injector type is able to produce. Ultimately, the shockwave structures in all ramp and flush wall cases emphasize the importance of employing shockwaves to condition downstream flow for enhanced mixing and combustion characteristics.

(vi) The efficiency of the combustor is solely reliant upon the quality and quantity of fuel-air mixing close to the injector. Due to the minimal residence time of fluid interaction in a given area of a combustor due to high fluid velocities, and the limited geometric constraints applied to scramjet designs to optimise weight management etc, effective mixing and rapid combustion is essential to achieving good levels of combustion, efficiently.

(vii) The flush wall injector cases presented highlight the importance of design optimisation and shockwave conditioning as the injection method embodies minimal mixing characteristics. The flush wall results indicate minimal exothermic behaviours as reflected by temperature contours, where significant ignition delay is observed.

(viii) The ramp cases, due to their intrusive presence in the flow field present the highest quality of combustion efficiency, with turbulent effects induced by their geometry inducing high energy rotational flows, enhancing downstream mixing greatly, as reflected in ramp injection temperature contours. The 12˚ and 18˚ ramp cases exhibit the highest quality and quantity of mixing, with flush wall cases promoting minimal observable mixing characteristics.

(ix) Velocity and temperature contours indicate significant recirculation zones in the cases of ramp injection, leading to elongated and stable streamwise regions of excited thermal activity.

(x) The flush wall 30 degrees and 80 degrees cases exhibit minimal mixing characteristics prior to reflected shockwave interaction, where the injected fuel is primarily introduced to the boundary layer. In all cases shock-induced mixing and combustion characteristics are observable, where flush wall injection is the primary beneficiary of the phenomena, leading to observable excited thermal regions far downstream of the combustor length. Temperature and H2O mass fractions indicate that ramp injection experience very good levels of combustion and isolated ignition regions prior to benefitting from shock-induced effects. For higher levels of combustion therefore, intrusive injection methods are required for optimal mixing and thrust generation.

(xi) The 12˚ ramp injector case indicates the best performance overall compared to the flush wall cases and the

higher inclination 18˚ ramp case. Compared to the flush wall injection method, the 12˚ ramp sees intense vortical mixing and excited thermal effects prior to shockwave interaction, where the 30˚ and 80˚ cases do not experience or benefit from turbulent mixing characteristics. The 12˚ ramp case, as emphasised by H_2O mass fraction contours, experiences adequate rotational mixing effects prior to a stable combustion region developed at the freestream and mixing layer boundary, which is further seen to be excited further by the reflected oblique shockwave.

(xii) The 18˚ ramp case, while experiencing greater vortical effects due to the elevation of fuel injection, experiences a mixing and combustive region closer to the boundary layer. Due to the early onset of intense turbulence and the high quality of mixing close to the boundary layer, the 18˚ ramp case experiences isolated combustion closer to the lower wall, leading to a reduction in the intensity of exothermic processes toward the modelled combustor exit.

There are several observations and recommendations that can be made following the research presented. The results obtained in the study emphasise the presence and significant effect of shockwave structures within the combustor. For all cases presented, particularly in the flush wall cases, the presence of shockwaves enhanced mixing of the fuel-air layer and induced combustion. For the flush wall cases, it is emphasised that combustive processes may not have been observed without the impingement of a strong reflected bow-shock due to the injection of hydrogen. In the ramp injector cases, while significant heat transfer and rotational flow behaviours are observable prior to shock-impingement, the utilisation of reflected shockwaves can still be significantly beneficial for stable combustion and enhanced mixing. The idea of a 'shock-generator' has been previously studied by Abdollahi et al. [29]. Enhanced combustive efficiency is proposed by utilising design-induced shockwaves to excite vortical and exothermic effects. As such, the method of shock-generation is recommended for further study to enhance flow path optimisation of scramjet combustors in the form of fixed or retractable ramps for thrust control. Another important area to consider in subsequent investigations is 3-dimensional simulation. This can successfully capture the characteristics of counter-rotating vortex pairs (CVPs) that are present when flow intrusions occur in the form of fuel injection or intrusive injector types whereby an injectant penetrating an oncoming freestream induces rotational vortices that diverge with downstream distance. The behaviour observed with CVPs occurs with flush wall injection, where vortical mixing enhancements and fuel-air diffusion would benefit the quality of results obtained. Efforts in these directions are currently underway and will be communicated imminently.

References

[1] J. Urzay, Supersonic combustion in air-breathing propulsion systems for hypersonic flight, *Annual Review of Fluid Mechanics,* Vol. 50, pp. 593-627, 2018.

[2] M. B. Gerdroodbary, 2020, *Scramjets: fuel mixing and injection systems*, Butterworth-Heinemann,

[3] T. G. Drozda, R. Baurle, CFD analysis of mixing characteristics of several fuel injectors at hypervelocity flow conditions, in *Proceeding of,* 4764.

[4] T. G. Drozda, R. Shenoy, E. L. Axdahl, R. A. Baurle, Numerical investigation and optimization of a flushwall injector for scramjet applications at hypervelocity flow conditions, in *Proceeding of,* 4196.

[5] Y. Bouazzi, A. B. Ali, L. Mostafa, A. K. Singh, S. Dixit, P. Sharma, H. Rajab, A. Eladeb, L. Kolsi, A. El-Shafay, Investigation of the injector configurations of ramp injection system for efficient hydrogen mixing inside the combustor of scramjet engine, *International Journal of Hydrogen Energy,* Vol. 143, pp. 527-536, 2025.

[6] S. S. Dharan, A. Vaidyanathan, D. SLN, Supersonic mixing characteristics of an internal cross-flow effervescent ramp injector, in *Proceeding of,* 3054.

[7] I. Omar, M. R. El-Sharkawy, R. Ali, P. K. Singh, H. Rajab, M. Ahmed, N. B. Ali, W. Rajhi, L. B. Said, S. A. Abodollahi, Usage of double injector for efficient mixing of the fuel behind the ramp injector at supersonic combustion chamber, *Scientific Reports,* Vol. 15, No. 1, pp. 1151, 2025.

[8] L. S. Jacobsen, S. D. Gallimore, J. A. Schetz, W. F. O'Brien, L. Goss, Improved aerodynamic-ramp injector in supersonic flow, *Journal of Propulsion and Power,* Vol. 19, No. 4, pp. 663-673, 2003.

[9] T. K. Swain, A. K. P, S. Kumar, Evaluation of fuel and air mixing in a scramjet engine using an asymmetric strut-based fuel injection using CFD, *Combustion Science and Technology,* Vol. 194, No. 5, pp. 898-918, 2022.

[10] E. Abdelhameed, K. Okamoto, Y. Watanabe, Numerical study on hydrogen mixing for different scramjet Engine combustion chamber configurations, in *Proceeding of,* International Exchange and Innovation Conference on Engineering & Sciences, pp.

[11] J. Hu, J. Chang, W. Bao, Q. Yang, J. Wen, Experimental study of a flush wall scramjet combustor equipped with strut/wall fuel injection, *Acta Astronautica,* Vol. 104, No. 1, pp. 84-90, 2014.

[12] H. Lingyun, B. Weigand, M. Banica, Effects of staged injection on supersonic mixing and combustion, *Chinese Journal of Aeronautics,* Vol. 24, No. 5, pp. 584-589, 2011.
[13] O. R. Kummitha, K. Pandey, Effect of wavy wall strut fuel injector on shock wave development and mixing enhancement of fuel and air for a scramjet combustor, *Journal of Computational Design and Engineering,* Vol. 8, No. 1, pp. 362-375, 2021.
[14] J. M. Donohue, J. C. McDaniel Jr, H. Haj-Hariri, Experimental and numerical study of swept ramp injection into a supersonic flowfield, *AIAA journal,* Vol. 32, No. 9, pp. 1860-1867, 1994.
[15] D. W. Bogdanoff, Advanced injection and mixing techniques for scramjet combustors, *Journal of Propulsion and Power,* Vol. 10, No. 2, pp. 183-190, 1994.
[16] P. Rubins, R. Bauer, Review of shock-induced supersonic combustion research and hypersonic applications, *Journal of Propulsion and Power,* Vol. 10, No. 5, pp. 593-601, 1994.
[17] G. Masuya, T. Komuro, A. Murakami, N. Shinozaki, A. Nakamura, M. Murayamall, K. Ohwaki, Ignition and combustion performance of scramjet combustors with fuel injection struts, *Journal of Propulsion and Power,* Vol. 11, No. 2, pp. 301-307, 1995.
[18] T. Mitani, N. Chinzei, T. Kanda, Reaction and mixing-controlled combustion in scramjet engines, *Journal of Propulsion and Power,* Vol. 17, No. 2, pp. 308-314, 2001.
[19] Z. B. Houria, K. Hajlaoui, S. A. Aminian, V. A. Musa, A. M. Sadeq, M. Shaban, W. Aich, K. Kriaa, Optimization strut-based fuel injection using multi-step hydrogen jets and air-assisted mixing in supersonic flow, *Scientific Reports*, 2026.
[20] E. H. Hirschel, W. Staudacher, M. Hornung, D. Kliche, *Basics of ramjet and scramjet propulsion*, in: *Elements of Hypersonic Airbreather Design and Development*, Eds., pp. 135-169: Springer, 2025.
[21] J. E. Matsson, 2022, *An introduction to ANSYS fluent 2022*, Sdc Publications,
[22] D. C. Wilcox, 1998, *Turbulence modeling for CFD*, DCW industries La Canada, CA,
[23] A. Fluent, Ansys Fluent Theory Guide, *ANSYS Inc*, 2011.
[24] H. Meicenheimer, E. Gutmark, C. Carter, D. Eklund, M. Gruber, A computational assessment of independent stage control of a cascade injector, in *Proceeding of,* 4863.
[25] J. Odam, A. Paull, Radical farming in scramjets, in *Proceeding of,* Springer, pp. 276-283.
[26] Q. Liu, D. Baccarella, W. Landsberg, A. Veeraragavan, T. Lee, Cavity flameholding in an optical axisymmetric scramjet in Mach 4.5 flows, *Proceedings of the combustion institute,* Vol. 37, No. 3, pp. 3733-3740, 2019.
[27] A. Ben-Yakar, R. K. Hanson, Cavity flame-holders for ignition and flame stabilization in scramjets: an overview, *Journal of propulsion and power,* Vol. 17, No. 4, pp. 869-877, 2001.
[28] T. Kouchi, C. P. Goyne, R. D. Rockwell, J. C. McDaniel, Focusing-schlieren visualization in a dual-mode scramjet, *Experiments in Fluids,* Vol. 56, No. 12, pp. 211, 2015.
[29] S. A. Abdollahi, M. Jafari, S. Aminian, M. Fattahi, P. Uyen, Fuel mixing enhancement of transverse coaxial air and fuel jet by upstream shock wave on in scramjet engines: numerical study, *Scientific Reports,* Vol. 13, No. 1, pp. 18501, 2023.